

Recovering Linear Causal Models with Latent Variables via Cholesky Factorization of Covariance Matrix

Yunfeng Cai, Xu Li, Minging Sun, Ping Li

Cognitive Computing Lab
Baidu Research
No.10 Xibeiwang East Road, Beijing 100193, China
10900 NE 8th St. Bellevue, Washington 98004, USA

{yunfengcai09, dongfangyixi, sunmingming01, pingli98}@gmail.com

Abstract

Discovering the causal relationship via recovering the directed acyclic graph (DAG) structure from the observed data is a well-known challenging combinatorial problem. When there are latent variables, the problem becomes even more difficult. In this paper, we first propose a DAG structure recovering algorithm, which is based on the Cholesky factorization of the covariance matrix of the observed data. The algorithm is fast and easy to implement and has theoretical guarantees for exact recovery. On synthetic and real-world datasets, the algorithm is significantly faster than previous methods and achieves the state-of-the-art performance. Furthermore, under the equal error variances assumption, we incorporate an optimization procedure into the Cholesky factorization based algorithm to handle the DAG recovering problem with latent variables. Numerical simulations show that the modified “Cholesky + optimization” algorithm is able to recover the ground truth graph in most cases and outperforms existing algorithms.

1 Introduction

Learning the causal relationships is a fundamental problem and has many applications in biology, machine learning, medicine, and economics. However, in many cases, not all causal variables relevant to the observed features have been measured. For example, in healthcare domains, there may be numerous unobserved factors such as gene expression; In financial markets, stock returns may be causally related but may also be confounded or mediated by a complicated network of unmeasured economic and political factors; Self-reported family history and diets may also leave out some important information.

Most causal discovery approaches focus on the situation without latent variables. For example, search-based algorithms (Chickering, 2002; Friedman and Koller, 2003; Teyssier and Koller, 2005; Aragam and Zhou, 2015; Ramsey et al., 2017; Tsamardinos et al., 2006; Lv et al., 2021; Ye et al., 2021) generally adopt a score (e.g., BIC score (Peters et al., 2014), Cholesky score (Ye et al., 2021), remove-fill score (Squires et al., 2020), Clustering Information Criterion (CIC) (Niu et al., 2022)) to measure the fitness of graphs over data and then search over the legal DAG (directed acyclic graph) space to find the structure that achieves the highest score. However, exhaustive search over the legal DAG space is infeasible when p is large (e.g., there are $4.1e^{18}$ DAGs for $p = 10$ (Sloane, 2003)). Those algorithms go in quest of a trade-off between performance and time complexity.

Topology order search algorithms (Ghoshal and Honorio, 2017, 2018; Chen et al., 2019; Gao et al., 2020; Park, 2020) decompose the DAG learning problem into two phases: (i) Topology order learning via conditional variance of the observed data; (ii) Graph estimation depends on the learned topology order. Those algorithms reduce the computation complexity into polynomial time and are guaranteed to recover the DAG structure under proper assumptions. Since Zheng *et al.* (Zheng et al., 2018) proposed an approach that converts the traditional combinatorial optimization problem into a continuous program, many methods (Ng et al., 2019; Yu et al., 2019; Lachapelle et al., 2020; Lee et al., 2020; Squires et al., 2020; Zheng et al., 2020; Zhu et al., 2021; Ng et al., 2022) have been proposed. To overcome the constraints of conventional methodologies, researchers have introduced algorithms that leverage reinforcement learning (Zhu et al., 2020; Wang et al., 2021) or flow-based techniques (Ren et al., 2021, 2022b,a; Ren and Li, 2022), aiming to mitigate the stringent assumptions inherent in traditional approaches.

Causal discovery with latent variables is less studied. The FCI (Spirtes et al., 1999), RFCI (Colombo et al., 2012), and ICD (Rohekar et al., 2021) methods can distinguish the observed variables and the latent variables that are confounders of the two observed ones and can recover up to a partial ancestral graph (PAG), which is an equivalence class of the true causal graph, even in the situation that the causal graph is able to exactly recovered. Some methods focus on special topology cases for non-Gaussian models, e.g., (Spearman, 1928; Hoyer et al., 2008b; Shimizu et al., 2009; Tashiro et al., 2014; Cai et al., 2019). Other works (Salehkaleybar et al., 2020; Xie et al., 2020) relax the special cases to more general non-Gaussian partially observable DAGs.

Contributions: This paper studies the linear causal models via Cholesky factorization:

1. For the case when all variables are observed, we propose a Cholesky factorization based method (namely, CDCF) to discover the causal structure. The time complexity of CDCF is $O(p^3)$, which is the fastest method so far. Here p is the number of nodes.
2. We show that CDCF is able to recover the DAG exactly, under standard assumptions. Sample complexity can be also obtained. We propose a novel algorithm (namely, CDCF⁺) to deal with the linear causal models with latent variables.
3. Numerical simulations show that CDCF and CDCF⁺ achieve the state-of-the-art performance.

Organization. Section 2 introduces the algorithm for linear causal models with exact recovery analysis. Section 3 gives the algorithm for the linear causal models with latent variables. Numerical results are provided in Section 4. Finally, Section 5 concludes the paper.

Notations. The symbol $\|\cdot\|$ stands for the Euclidean norm of a vector or the spectral norm of a matrix. For a matrix $\mathbf{A} \in \mathbb{R}^{m \times n}$, \mathbf{A}_{ij} , $\mathbf{A}_{i,:}$, $\mathbf{A}_{:,j}$ stand for the (i, j) entry, the i th row and j th column of \mathbf{A} , respectively. Let $\underline{i} = [i_1, \dots, i_k]$, $\underline{j} = [j_1, \dots, j_\ell]$ be subsets of $[1, \dots, m]$, $[1, \dots, n]$, respectively. $\mathbf{A}_{\underline{i},:}$, $\mathbf{A}_{:, \underline{j}}$, $\mathbf{A}_{\underline{i}, \underline{j}}$ stand for the sub-matrices of \mathbf{A} consisting of all rows in \underline{i} , columns in \underline{j} , and the intersection of rows in \underline{i} and columns in \underline{j} , respectively. The symbol $\|\mathbf{A}\|_1$, $\|\mathbf{A}\|_{\max}$, $\|\mathbf{A}\|_{2,\infty}$ stand for ℓ_1 -norm, max-norm and 2-infinity norm, respectively, i.e., $\|\mathbf{A}\|_1 = \sum_{i,j} |\mathbf{A}_{ij}|$, $\|\mathbf{A}\|_{\max} = \max_{i,j} |\mathbf{A}_{ij}|$, $\|\mathbf{A}\|_{2,\infty} = \max_i \|\mathbf{A}_{i,:}\|$.

2 Recover Linear Causal Models via Cholesky Factorization

2.1 Preliminaries and Assumptions

Assume that the observed data is entailed by a DAG $\mathcal{G} = (V, E)$, where V , E are the sets of nodes and edges, respectively. Each node v_i corresponds to a random variable X_i . The data matrix is given by $\mathbf{X} = [\mathbf{x}_1, \dots, \mathbf{x}_p] \in \mathbb{R}^{n \times p}$, where $p = |V|$, \mathbf{x}_i is consisted of n i.i.d observations of the random variable X_i , for $k = 1, \dots, p$. The joint distribution of \mathbf{X} is $P(\mathbf{X}) = \prod_{i=1}^p P(X_i | \text{Pa}_{\mathcal{G}}(X_i))$, where $\text{Pa}_{\mathcal{G}}(X_i) := \{X_j | (v_i, v_j) \in E\}$ is the set of parents of node X_i .

Given \mathbf{X} , we seek to recover the latent DAG topology structure for the joint probability distribution (Hoyer et al., 2008a; Peters et al., 2017). Generally, \mathbf{X} is modeled via a structural equation model (SEM) with the form

$$X_i = f_i(\text{Pa}_{\mathcal{G}}(X_i)) + N_i, \quad i = 1, \dots, p,$$

where f_i is an arbitrary function representing the relation between X_i and its parents, N_i is the jointly independent noise variable.

In this paper, we focus on the linear SEM defined by

$$X_i = [X_1, \dots, X_p] \mathbf{w}_i + N_i, \quad i = 1, \dots, p, \quad (1)$$

where $\mathbf{w}_i \in \mathbb{R}^p$ is a weighted column vector. Let $\mathbf{W} = [\mathbf{w}_1, \dots, \mathbf{w}_p] \in \mathbb{R}^{p \times p}$ be the weighted adjacency matrix, $\mathbf{N} = [\mathbf{n}_1, \dots, \mathbf{n}_p] \in \mathbb{R}^{n \times p}$ be the noise matrix, where \mathbf{n}_i is n i.i.d observations of the noise variable N_i . The linear SEM model (1) can be rewritten as

$$\mathbf{X} = \mathbf{XW} + \mathbf{N}. \quad (2)$$

As proposed in Nicholson (1975); McKay et al. (2004), a graph is DAG if and only if the corresponding weighted adjacent matrix \mathbf{W} can be decomposed into

$$\mathbf{W} = \mathbf{PTP}^T, \quad (3)$$

where \mathbf{P} is a permutation matrix, \mathbf{T} is a strict upper triangular matrix, i.e., $\mathbf{T}_{ij} = 0$ for all $i \geq j$.

Layer Decomposition The *layer decomposition* (Gao et al., 2020) of a DAG can be obtained as follows: let $\mathcal{L}_0 := \emptyset$, $\mathcal{A}_j := \cup_{m=0}^j \mathcal{L}_m$; for $j > 0$, \mathcal{L}_j is the set of all source nodes in the subgraph formed by removing the nodes in \mathcal{A}_{j-1} .

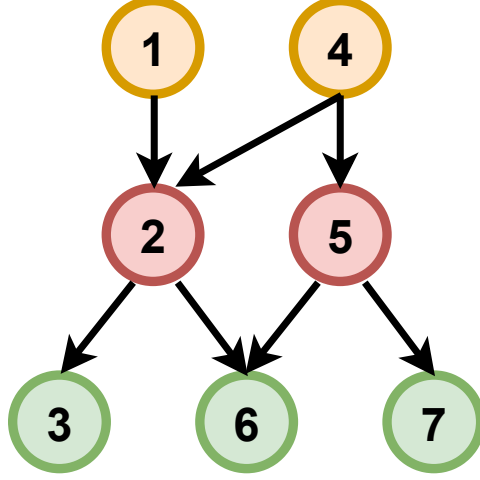


Figure 1: Three-layer DAG

For example, the graph in Figure 1 has three layers with $\mathcal{L}_1 = \{node1, node4\}$, $\mathcal{L}_2 = \{node2, node5\}$, $\mathcal{L}_3 = \{node3, node6, node7\}$. Furthermore, the adjacent matrix \mathbf{W} can be given by

$$\mathbf{W} = \begin{bmatrix} 0 & 1 & 0 & 0 & 0 & 0 & 0 \\ 0 & 0 & 1 & 0 & 0 & 1 & 0 \\ 0 & 0 & 0 & 0 & 0 & 0 & 0 \\ 0 & 1 & 0 & 0 & 1 & 0 & 0 \\ 0 & 0 & 0 & 0 & 0 & 1 & 1 \\ 0 & 0 & 0 & 0 & 0 & 0 & 0 \\ 0 & 0 & 0 & 0 & 0 & 0 & 0 \end{bmatrix}.$$

Let

$$\mathbf{P} = \begin{bmatrix} 1 & 0 & 0 & 0 & 0 & 0 & 0 \\ 0 & 0 & 1 & 0 & 0 & 0 & 0 \\ 0 & 0 & 0 & 0 & 1 & 0 & 0 \\ 0 & 1 & 0 & 0 & 0 & 0 & 0 \\ 0 & 0 & 0 & 1 & 0 & 0 & 0 \\ 0 & 0 & 0 & 0 & 0 & 1 & 0 \\ 0 & 0 & 0 & 0 & 0 & 0 & 1 \end{bmatrix}, \quad \mathbf{T} = \begin{bmatrix} 0 & 0 & 1 & 0 & 0 & 0 & 0 \\ 0 & 0 & 1 & 1 & 0 & 0 & 0 \\ 0 & 0 & 0 & 0 & 1 & 1 & 0 \\ 0 & 0 & 0 & 0 & 0 & 1 & 1 \\ 0 & 0 & 0 & 0 & 0 & 0 & 0 \\ 0 & 0 & 0 & 0 & 0 & 0 & 0 \\ 0 & 0 & 0 & 0 & 0 & 0 & 0 \end{bmatrix},$$

(3) holds. Note that \mathbf{T} is a strict block upper triangular matrix. For a general r -layer DAG, there exists a permutation matrix \mathbf{P} such that (3) holds with \mathbf{T} having a strict block upper triangular form:

$$\mathbf{T} = [\mathbf{T}_{ij}] = \begin{bmatrix} 0 & \mathbf{T}_{12} & \mathbf{T}_{13} & \dots & \mathbf{T}_{1r} \\ 0 & 0 & \mathbf{T}_{23} & \dots & \mathbf{T}_{2r} \\ 0 & 0 & & \ddots & \vdots \\ \vdots & & & \ddots & \mathbf{T}_{r-1,r} \\ 0 & \dots & \dots & 0 & 0 \end{bmatrix}, \quad (4)$$

where $\mathbf{T}_{ij} \in \mathbb{R}^{p_i \times p_j} = 0$ for $1 \leq i \leq j \leq r$, p_i equals the number of nodes in \mathcal{L}_i for $1 \leq i \leq r$, each column of $\mathbf{T}_{i,i+1}$ is nonzero (otherwise, the corresponding node belongs to the i th layer). The decomposition (3) with \mathbf{T} having the strict block upper triangular form (4) is *unique* up to all within layer permutations (the Markov equivalence class).

Throughout the rest of this paper, we will make the following assumptions:

A1 The noise variables are all centered, uncorrelated, and have finite variances, i.e.,

$$\mathbb{E}(N_i) = 0, \quad \boldsymbol{\Sigma}_{nn} = [\mathbb{E}(N_i N_j)] = \text{diag}(\sigma_1^2, \dots, \sigma_p^2) < \infty.$$

A2 Let the weighted adjacency matrix \mathbf{W} be decomposed as in (3) with \mathbf{T} having the block diagonal form (4). Assume

$$\Delta = \min_{\substack{j < k \\ i_s \in \mathcal{I}_j, i_t \in \mathcal{I}_k}} \sigma_{i_t}^2 - \sigma_{i_s}^2 + \|\mathbf{U}\|_{i_s:i_{t-1}, i_t}^2 > 0,$$

where

$$\dot{\mathbf{i}} = [i_1, \dots, i_p] = [1, \dots, p] \mathbf{P}, \quad (5a)$$

$$\mathcal{I}_j = \left\{ \sum_{i=1}^{j-1} p_i + 1, \dots, \sum_{i=1}^j p_i \right\} \quad \text{for } 1 \leq j \leq r, \quad (5b)$$

$$\mathbf{U} = \text{diag}(\sigma_{i_1}, \dots, \sigma_{i_p}) (\mathbf{I} - \mathbf{T})^{-1}. \quad (5c)$$

Assumption **A2** is essentially the same as the identifiability condition in Park (2020, Thm. 2) and Gao et al. (2020, Thm. B2).

In the rest of this section, we assume that there are no latent variables. The case when latent variables exist will be discussed in Section 3.

2.2 Algorithm

It follows from (2), (3) and (5a) that

$$[X_{i_1}, \dots, X_{i_p}] = [N_{i_1}, \dots, N_{i_p}] (\mathbf{I} - \mathbf{T})^{-1}. \quad (6)$$

Using (6) and **A1**, we have

$$[\boldsymbol{\Sigma}_{xx}]_{\dot{\mathbf{i}}, \dot{\mathbf{i}}} = (\mathbf{I} - \mathbf{T})^{-\text{T}} [\boldsymbol{\Sigma}_{nn}]_{\dot{\mathbf{i}}, \dot{\mathbf{i}}} (\mathbf{I} - \mathbf{T})^{-1} = \mathbf{U}^{\text{T}} \mathbf{U}, \quad (7)$$

where \mathbf{U} is defined in (5c). Note that \mathbf{U} is upper triangular, hence (7) is simply the Cholesky factorization of the permuted covariance matrix $[\boldsymbol{\Sigma}_{xx}]_{\dot{\mathbf{i}}, \dot{\mathbf{i}}}$. The task becomes to find the permutation $\dot{\mathbf{i}} = [i_1, \dots, i_p]$ and an upper triangular matrix $\tilde{\mathbf{U}}$ such that $\tilde{\mathbf{U}}^{\text{T}} \tilde{\mathbf{U}}$ is a good approximation of $[\boldsymbol{\Sigma}_{xx}]_{\dot{\mathbf{i}}, \dot{\mathbf{i}}}$.

Let $\tilde{\boldsymbol{\Sigma}}_{xx}$ be an estimator for the population covariance matrix $\boldsymbol{\Sigma}_{xx}$. Assume that $\dot{\mathbf{i}}_{k-1} := [i_1, \dots, i_{k-1}]$ and $\tilde{\mathbf{U}}_{k-1} := \tilde{\mathbf{U}}_{1:k-1, 1:k-1}$ are settled, and we have

$$[\tilde{\boldsymbol{\Sigma}}_{xx}]_{\dot{\mathbf{i}}_{k-1}, \dot{\mathbf{i}}_{k-1}} = \tilde{\mathbf{U}}_{k-1}^{\text{T}} \tilde{\mathbf{U}}_{k-1}. \quad (8)$$

Next, we show how to find i_k and $\tilde{\mathbf{U}}_k$. For the time being, let us assume i_k is known, we show how to compute the last column of $\tilde{\mathbf{U}}_k$. Let $\tilde{\mathbf{U}}_k = \begin{bmatrix} \tilde{\mathbf{U}}_{k-1} & \boldsymbol{\beta}_k \\ 0 & \alpha_k \end{bmatrix}$ with $\alpha_k \in \mathbb{R}$, $\boldsymbol{\beta}_k \in \mathbb{R}^{k-1}$. Then using (8), we get

$$[\tilde{\boldsymbol{\Sigma}}_{xx}]_{\dot{\mathbf{i}}_k, \dot{\mathbf{i}}_k} = \tilde{\mathbf{U}}_k^{\text{T}} \tilde{\mathbf{U}}_k = \begin{bmatrix} \tilde{\mathbf{U}}_{k-1}^{\text{T}} \tilde{\mathbf{U}}_{k-1} & \tilde{\mathbf{U}}_{k-1}^{\text{T}} \boldsymbol{\beta}_k \\ \boldsymbol{\beta}_k^{\text{T}} \tilde{\mathbf{U}}_{k-1} & \alpha_k^2 + \|\boldsymbol{\beta}_k\|^2 \end{bmatrix}.$$

Algorithm 1 Causal Discovery via Cholesky Factorization (CDCF)

- 1: **input:** The covariance matrix $\tilde{\Sigma}_{xx} \in \mathbb{R}^{p \times p}$.
 - 2: **output:** A permutation $\tilde{\mathbf{P}}$ and an upper triangular matrix $\tilde{\mathbf{U}}_p^{-1}$.
 - 3: Set $\underline{\mathbf{i}} = [1, 2, \dots, p]$;
 - 4: $\ell = \operatorname{argmin}_{1 \leq j \leq p} [\tilde{\Sigma}_{xx}]_{i_j, i_j}$, exchange i_1 and i_ℓ in $\underline{\mathbf{i}}$;
 - 5: Set $\alpha_1 = \sqrt{[\tilde{\Sigma}_{xx}]_{i_1, i_1}}$, $\tilde{\mathbf{U}}_1 = \alpha_1$, $\tilde{\mathbf{U}}_1^{-1} = \frac{1}{\alpha_1}$;
 - 6: **for** $k = 2, 3, \dots, p$ **do**
 - 7: **for** $j = k, k + 1, \dots, p$ **do**
 - 8: Compute α_j, β_j via (9);
 - 9: **end for**
 - 10: $\ell = \operatorname{argmin}_{k \leq j \leq p} \alpha_j^2$, exchange i_k and i_ℓ in $\underline{\mathbf{i}}$;
 - 11: $\tilde{\mathbf{U}}_k = \begin{bmatrix} \tilde{\mathbf{U}}_{k-1} & \beta_\ell \\ 0 & \alpha_\ell \end{bmatrix}$, $\tilde{\mathbf{U}}_k^{-1} = \begin{bmatrix} \tilde{\mathbf{U}}_{k-1}^{-1} & -\frac{1}{\alpha_\ell} \tilde{\mathbf{U}}_{k-1}^{-1} \beta_\ell \\ 0 & \frac{1}{\alpha_\ell} \end{bmatrix}$;
 - 12: **end for**
 - 13: Set $\tilde{\mathbf{P}} = \mathbf{I}(:, \underline{\mathbf{i}})$, \mathbf{I} is the order p identity matrix.
-

It follows immediately that

$$\beta_k = \tilde{\mathbf{U}}_{k-1}^{-\text{T}} [\tilde{\Sigma}_{xx}]_{\underline{\mathbf{i}}_{k-1}, i_k}, \quad \alpha_k = \sqrt{[\tilde{\Sigma}_{xx}]_{i_k, i_k} - \|\beta_k\|^2}. \quad (9)$$

By (9), once i_k is settled, we can obtain the last column of $\tilde{\mathbf{U}}_k$. The task remains to select i_k from $\{1, \dots, p\} \setminus \{i_1, \dots, i_{k-1}\}$. In this paper, we compute α_j and β_j by (9) for all possible j ($i_j \in \{1, \dots, p\} \setminus \{i_1, \dots, i_{k-1}\}$). Then determine i_k by

$$i_k = \operatorname{argmin}_{k \leq j \leq p} \alpha_j^2. \quad (10)$$

The intuition behind (10) is that α_j^2 is the empirical conditional variance of X_j , thus, \mathbf{X}_{i_k} is chosen as the one with the smallest conditional variance. One may also consider some alternatives, say choose i_k via the sparsity of $\tilde{\mathbf{U}}_{k-1}^{-1} \beta_k$, or take both the sparsity and the conditional variance into account.

The overall algorithm is summarized in Algorithm 1. Recall (5c) and denote $\mathbf{A} = \operatorname{diag}(\alpha_1, \dots, \alpha_p)$, we can obtain the adjacent matrix $\tilde{\mathbf{W}}$ as follows:

$$\tilde{\mathbf{W}} = [\operatorname{TRIU}(\operatorname{TRUNCATE}(\tilde{\mathbf{U}}_p^{-1} \mathbf{A}, \omega))]_{\operatorname{REV}(\underline{\mathbf{i}}), \operatorname{REV}(\underline{\mathbf{i}})}, \quad (11)$$

that is, we truncate $\tilde{\mathbf{U}}_p^{-1} \mathbf{A}$ element-wisely, then take its strict upper triangular part (denoted by “TRIU”) and re-permute the predicted adjacent matrix back to the original order according to the permutation order $\underline{\mathbf{i}}$. Here $\omega > 0$ is a truncate threshold: a number less than ω in absolute value is truncated to zero; otherwise, it remains unchanged.

Time Complexity. On line 8, we only need to compute the last entry of β_j at the cost of $\mathcal{O}(p)$ at worst since the other entries are available from the previous steps. Therefore, the overall time complexity of Algorithm 1 is $\mathcal{O}(p^3)$. Additionally, the inner loop (lines 7 to 9) can be made in parallel, which makes the algorithm friendly to run on GPU and suitable for large scale calculations. It is worth mentioning here that the time complexity for the computation of $\tilde{\Sigma}_{xx}$ is not included here since we take it as an overhead of CDCF.

Remark 1. *Algorithm 1 differs from other methods (e.g., Ghoshal and Honorio (2017, 2018); Chen et al. (2019); Gao et al. (2020); Park (2020)) in that, it combines the topology order search stage and the graph estimation stage together, rather than two-stage: first topology order search then graph estimation, which leads to the reduction of the time complexity.*

2.3 Exact Recovery

In this section, we show that Algorithm 1 is able to exactly recover the ordering and the graph structure. All proofs are given in the appendix.

Theorem 2.1 (Exact recovery of the ordering). *For the linear SEM model (1), assume (3), A1 and A2. Let $\tilde{\Sigma}_{xx}$ be an estimator for $\Sigma_{xx} = [\mathbb{E}(X_j X_k)]$ and $\max_i |[\Sigma_{xx}]_{ii} - [\tilde{\Sigma}_{xx}]_{ii}| \leq \epsilon_d$ for some $\epsilon_d > 0$. If $\epsilon_d < \frac{\Delta}{4}$, Algorithm 1 recovers the ordering exactly.*

Sample complexity for the ordering. According to Theorem 2.1, we can obtain the sample complexity for the exact recovery of the ordering by $\max_i ||[\Sigma_{xx}]_{ii} - [\tilde{\Sigma}_{xx}]_{ii}|| \leq \Delta/4$. Specifically, X_i is a linear combination of N_i 's and $\mathbb{E}(X_i) = 0$, $\text{Var}(X_i) = [\Sigma_{xx}]_{ii}$. Then we can obtain the sample complexity $\mathcal{O}(\log(p/\epsilon)\mathcal{M}^2)$, where $\mathcal{M} = \max_i [\Sigma_{xx}]_{ii}$. The proof can be found in Appendix. In the following Table 1, we compare the sample complexity with others'.

Table 1: Sample complexity for the ordering. The last column represents the \mathcal{O} complexity of the sample number n that makes the algorithm recover the DAG with probability at least $1 - \epsilon$, p is the nodes number, r represents the level of the graph, q is the maximum in-degree, d is the maximum total degree, m represents the m 'th moment bounded noise, $\mathcal{M} = \max_i [\Sigma_{xx}]_{ii}$, $g(x) = x/\log x$ (g^{-1} exists when $x > 3$ and it holds $g^{-1}(x) > x$).

Algorithm	Data	Function	Noise Type	\mathbf{X}	Sample Complexity
NPVAR Gao et al. (2020)	-	(Non)-linear Lip-continuous	-	-	$\mathcal{O}((rp/\epsilon)^{1+p/2})$
EV Chen et al. (2019)	$n > p$	Linear	Sub-Gaussian	$\lambda_{\min} > 0$	$\mathcal{O}(p^2 \log(p/\epsilon)\mathcal{M}^2)$
	$n < p$	Linear	Sub-Gaussian	$\lambda_{\min} > 0$	$\mathcal{O}(q^2 \log(p/\epsilon)\mathcal{M}^2)$
LISTEN Ghoshal and Honorio (2018)	-	Linear	Sub-Gaussian	-	$\mathcal{O}(d^4 \log(\frac{p}{\sqrt{\epsilon}})\mathcal{M}^2)$
	-	Linear	Bounded moment	-	$\mathcal{O}(d^4 (\frac{p^2}{\epsilon})^{1/m} \mathcal{M}^2)$
US Park (2020)	$n > p$	Linear	Gaussian	$\lambda_{\min} > 0$ $\lambda_{\max} < \infty$	$g^{-1}(\mathcal{O}(\log(p/\epsilon)\mathcal{M}^2))$
CDCF (ours)	-	Linear	-	-	$\mathcal{O}(\log(p/\epsilon)\mathcal{M}^2)$

Theorem 2.2 (Exact recovery of the structure). *Follow the notations and assumptions in Theorem 2.1. Denote*

$$\mu = \|\mathbf{I} - \mathbf{T}\|_{2,\infty} \|\mathbf{I} - \mathbf{T}^T\|_{2,\infty}, \quad \rho = \frac{\max_i \sigma_i}{\min_i \sigma_i^2}, \quad \omega = \min_{\mathbf{T}_{ij} \neq 0} |\mathbf{T}_{ij}|.$$

Assume $\|\Sigma_{xx} - \tilde{\Sigma}_{xx}\| \leq \epsilon_2$ for some $\epsilon_2 > 0$. If $\epsilon_2 \lesssim \frac{\omega^2}{8\rho^2\mu^2}$, then Algorithm 1 is able to recover the graph structure exactly.

Sample complexity for the graph structure. The sample complexity for the exact recovery of the graph structure can be established via $\|\Sigma_{xx} - \tilde{\Sigma}_{xx}\| \lesssim \frac{\omega^2}{8\rho^2\mu^2}$. For example, when the noise is sub-Gaussian, it holds with probability at least $1 - 2\exp(-ct^2)$ that

$$\|\tilde{\Sigma}_{xx} - \Sigma_{xx}\| \leq \|(\mathbf{I} - \mathbf{T})^{-1}\|^2 \max\{\delta, \delta^2\},$$

where $\delta = C\sqrt{\frac{p}{n}} + \frac{t}{\sqrt{n}}$, c and C are two constants. For simplicity, let $\delta \geq 1$. By calculations, we know that w.p. $\geq 1 - \epsilon$ it holds $\|\Sigma_{xx} - \tilde{\Sigma}_{xx}\| \lesssim \frac{\omega^2}{8\rho^2\mu^2}$ for $n = \mathcal{O}((p + \log \frac{1}{\epsilon})\rho^2\mu^2\|(\mathbf{I} - \mathbf{T})^{-1}\|^2/\omega^2)$. Sample complexities for other distributions of the noise can be obtained similarly.

3 Learning Linear Causal Models with Latent Variables

In this section, we study the effects of latent variables, then present an algorithm to recover them.

3.1 The Effects of Latent Variables

When there are latent variables, the covariance matrix of the observed variables is essentially a principal submatrix of the overall covariance matrix. To get a clue on how the Cholesky factor changes, we consider the case when there is one latent variable.

Let $\Sigma_+ = \begin{bmatrix} \Sigma_{11} & \mathbf{x} & \Sigma_{12} \\ \mathbf{x}^T & d^2 & \mathbf{y}^T \\ \Sigma_{12}^T & \mathbf{y} & \Sigma_{22} \end{bmatrix}$ be a symmetric positive definite matrix, where $\mathbf{x} \in \mathbb{R}^{p_1}$, $\mathbf{y} \in \mathbb{R}^{p_2}$, $\Sigma_{11} \in \mathbb{R}^{p_1 \times p_1}$, $\Sigma_{22} \in \mathbb{R}^{p_2 \times p_2}$. Let the Cholesky factorization of Σ_+ be $\Sigma_+ = \mathbf{U}_+^T \mathbf{U}_+$, where $\mathbf{U}_+ = \begin{bmatrix} \mathbf{U}_{11} & \hat{\mathbf{x}} & \mathbf{U}_{12} \\ 0 & \hat{d} & \hat{\mathbf{y}}^T \\ 0 & 0 & \hat{\mathbf{U}}_{22} \end{bmatrix}$, $\mathbf{U}_{11} \in \mathbb{R}^{p_1 \times p_1}$ and $\hat{\mathbf{U}}_{22} \in \mathbb{R}^{p_2 \times p_2}$ be both upper triangular. By simple calculations, we have

$$\hat{\mathbf{x}} = \mathbf{U}_{11}^{-T} \mathbf{x}, \hat{d} = \sqrt{d^2 - \|\hat{\mathbf{x}}\|^2}, \hat{\mathbf{y}} = \frac{1}{\hat{d}}(\mathbf{y} - \mathbf{U}_{12}^T \hat{\mathbf{x}}). \quad (12)$$

Denote $\mathbf{v} = \mathbf{U}_{11}^{-1} \hat{\mathbf{x}}$, $\mathbf{w} = \hat{\mathbf{U}}_{22}^{-T} \hat{\mathbf{y}}$. It also holds that

$$\mathbf{U}_+^{-1} = \begin{bmatrix} \mathbf{U}_{11}^{-1} & -\frac{1}{\hat{d}}\mathbf{v} & \frac{1}{\hat{d}}\mathbf{v}\mathbf{w}^T - \mathbf{U}_{11}^{-1}\mathbf{U}_{12}\hat{\mathbf{U}}_{22}^{-1} \\ 0 & \frac{1}{\hat{d}} & -\frac{1}{\hat{d}}\mathbf{w}^T \\ 0 & 0 & \hat{\mathbf{U}}_{22}^{-1} \end{bmatrix}. \quad (13)$$

Now we remove the $p_1 + 1$ st row and the corresponding column of Σ_+ , we get $\Sigma = \begin{bmatrix} \Sigma_{11} & \Sigma_{12} \\ \Sigma_{12}^T & \Sigma_{22} \end{bmatrix}$. For the Cholesky factor of Σ , we have the following results.

Proposition 1. Let the Cholesky factorization of Σ be $\Sigma = \mathbf{U}^\top \mathbf{U}$. It holds that

(a) \mathbf{U} can be given by $\mathbf{U} = \begin{bmatrix} \mathbf{U}_{11} & \mathbf{U}_{12} \\ 0 & \mathbf{U}_{22} \end{bmatrix}$, where \mathbf{U}_{22} satisfies

$$\mathbf{U}_{22}^\top \mathbf{U}_{22} = \widehat{\mathbf{U}}_{22}^\top \widehat{\mathbf{U}}_{22} + \widehat{\mathbf{y}} \widehat{\mathbf{y}}^\top. \quad (14)$$

(b) Let the Cholesky factorization of $\mathbf{I} + \mathbf{w}\mathbf{w}^\top$ be $\mathbf{I} + \mathbf{w}\mathbf{w}^\top = \mathbf{L}^\top \mathbf{L}$. Then \mathbf{U}^{-1} can be given by

$$\mathbf{U}^{-1} = \begin{bmatrix} \mathbf{U}_{11}^{-1} & -\mathbf{U}_{11}^{-1} \mathbf{U}_{12} \mathbf{U}_{22}^{-1} \\ 0 & \mathbf{U}_{22}^{-1} \end{bmatrix}, \quad \mathbf{U}_{22}^{-1} = \widehat{\mathbf{U}}_{22}^{-1} \mathbf{L}^{-1}. \quad (15)$$

(c) The k th diagonal entry of \mathbf{U}_{22} can be given by

$$[\mathbf{U}_{22}]_{kk} = \sqrt{(1 + \|\mathbf{w}_{1:k}\|^2)/(1 + \|\mathbf{w}_{1:k-1}\|^2)} [\widehat{\mathbf{U}}_{22}]_{kk}.$$

Proposition 1 (a) tells that the (1, 1) and (1, 2) blocks of \mathbf{U} are the same as the (1, 1) and (1, 3) blocks of \mathbf{U}_+ , respectively. In addition, (14) is a rank-1 update of Cholesky factorization. Proposition 1 (b) tells how the blocks of \mathbf{U}^{-1} relate with the blocks of \mathbf{U}_+^{-1} . The (1, 1) block of \mathbf{U}^{-1} is the same as the (1, 1) block of \mathbf{U}_+^{-1} . Recall that \mathbf{v} and \mathbf{w} determine the in-going and out-going edges of the $p_1 + 1$ st node, respectively, we expect \mathbf{v} and \mathbf{w} to be sparse. For all $1 \leq i < j < p_2$, $\mathbf{G}_{ij} \neq 0$ if and only if $\mathbf{w}_i \mathbf{w}_j \neq 0$. Hence \mathbf{G} (also its \mathbf{G}^{-1}) are sparse. We thus claim that the (1, 2) block of \mathbf{U}^{-1} can be obtained from the (1, 3) block of \mathbf{U}_+^{-1} by a sparse rank-1 update followed by a sparse matrix multiplication; the (2, 2) block of \mathbf{U}^{-1} can be obtained from the (3, 3) block of \mathbf{U}_+^{-1} by a sparse matrix multiplication. Proposition 1 (c) tells that whenever $\mathbf{w}_k \neq 0$, $[\mathbf{U}_{22}]_{kk} > [\widehat{\mathbf{U}}_{22}]_{kk}$ since $\frac{1 + \|\mathbf{w}_{1:k}\|^2}{1 + \|\mathbf{w}_{1:k-1}\|^2} > 1$. This indicates the variance of the child node becomes larger when its parent nodes are missing.

According to Proposition 1 and the discussion above, we may make the following claim:

- **C1** The (1, 2) and (2, 2) blocks of \mathbf{U}^{-1} become denser compared with the (1, 3) and (3, 3) blocks of \mathbf{U}_+^{-1} ;
- **C2** The variance for the child node of latent nodes becomes larger.

In order to recover DAG with latent variables, we have to detect the latent variables and identify their in-going and out-going edges. In this paper, we propose to detect latent variables via **C2** and identify in-going and out-going edges via **C1**. Note that **C2** alone is insufficient to detect latent variables since we only know the variance becomes larger. Thus, we make an equi-variance assumption to simplify the problem:

A3 The noise variables are all centered, uncorrelated and have equal variance σ^2 .

Remark 2. The essence of detecting latent variables is to determine where a latent node is missing and how it is connected to other nodes. To do so, one need to carefully design some criterion: whenever the criterion is violated, there is latent nodes. **A3** is perhaps the simplest criterion to accomplish the task. One may also consider exploring various alternatives, such as employing graph structures to refine the criterion. This approach might involve focusing on the sparsity pattern of the graph or examining the in-degree and out-degree of the nodes within the graph.

3.2 Algorithm

To proceed, we assume an estimation $\hat{\sigma}$ for σ in **A3** is available. This assumption is not restrictive since when a root node is observed, we can estimate $\hat{\sigma}$ via the sample variance of the root node.

At beginning, we observe $q < p$ nodes. Input $\tilde{\Sigma}_{xx} \in \mathbb{R}^{q \times q}$ into Algorithm 1, then it works as there were no latent variables until it encounters a child of latent variables. So, we may detect a latent variable when we find a diagonal entry of \tilde{U}_q larger than $\hat{\sigma}$, then we may determine its connection with other nodes via a sparse encouraging optimization problem. The above procedure can be used repeatedly to handle the case when there are multiple latent variables.

Next, we present the flowchart of the algorithm:

- **S1** Perform Algorithm 1 with input $\tilde{\Sigma}_{xx} \in \mathbb{R}^{q \times q}$, output \tilde{P} and \tilde{U}_q^{-1} .
- **S2** Check the diagonal entries of \tilde{U}_q^{-1} : if all entries are approximately $\frac{1}{\hat{\sigma}}$, then there is no (identifiable) latent variable; otherwise, find the first entry that is not approximately $\frac{1}{\hat{\sigma}}$ and let it be the j th.
- **S3** Insert a variable between $j - 1$ st and j th variables and determine its connections with others.
- **S4** Update $\tilde{\Sigma}_{xx}$ by appending one row and column to it, then go to step **S1** to repeat.

In what follows we give details for **S3** and **S4**. Define

$$\begin{aligned} \mathbf{U}(\mathbf{S}) &:= \hat{\sigma}(\mathbf{I} - \mathbf{S})^{-1}, \quad \mathbf{C}(\mathbf{S}) := \mathbf{U}(\mathbf{S})^T \mathbf{U}(\mathbf{S}), \\ \mathbf{S} \in \mathbb{U}_q &:= \{\mathbf{U} \in \mathbb{R}^{q \times q} \mid \mathbf{U}_{ij} = 0 \text{ for all } i > j\}. \end{aligned} \quad (16)$$

Let $\mathbf{i} = [1, \dots, q] \tilde{P}$ and we parameterize the Cholesky factor of $[\tilde{\Sigma}_{xx}]_{\mathbf{i}, \mathbf{i}}$ by $\mathbf{U}(\mathbf{S})$, with $\mathbf{S} \in \mathbb{U}_q$. Note that all diagonal entries of $\mathbf{U}(\mathbf{S})$ are $\hat{\sigma}$. The reason for having such a requirement is that after inserting a variable, we expect that the variances of all variables are approximately σ^2 . Note that \mathbf{S} should be sparse, and the resulting covariance matrix should be close to the observed covariance matrix. We thus determine \mathbf{S} by

$$\min_{\mathbf{S} \in \mathbb{U}_q} \|[\mathbf{C}(\mathbf{S})]_{\mathbf{j}^c, \mathbf{j}^c} - [\tilde{\Sigma}_{xx}]_{\mathbf{i}^c, \mathbf{i}^c}\|_F^2 + \mu \|\mathbf{S}\|_1, \quad (17)$$

where \mathbf{i}^c and \mathbf{j}^c are two index sets that pick all observed indices of $\tilde{\Sigma}_{xx}$ and $\mathbf{C}(\mathbf{S})$, respectively, $\mu \geq 0$ is a parameter.

Let \mathbf{S} be the solution to (17). We compute $\mathbf{C}(\mathbf{S})$ by (16), then update $\tilde{\Sigma}_{xx}$ as follows:

$$\tilde{\Sigma}_{xx} = \begin{bmatrix} \tilde{\Sigma}_{xx} & \mathbf{z} \\ \mathbf{z}^T & d^2 \end{bmatrix}, \quad (18)$$

where $\mathbf{z} = [\mathbf{x}^T, \mathbf{y}^T]^T$ with $\mathbf{x} = [\mathbf{C}(\mathbf{S})]_{1:j-1, j}$ and $\mathbf{y} = [\mathbf{C}(\mathbf{S})]_{j+1:q, j}$, $d^2 = [\mathbf{C}(\mathbf{S})]_{j, j}$.

The detailed algorithm is summarized in Algorithm 2. On input, ζ is a threshold to determine if the diagonal entries of \tilde{U}_q^{-1} are approximately $\frac{1}{\hat{\sigma}}$, μ is the sparsity encouraging parameter used in (17). Line 4, $\#\mathbf{j}$ stands for the number of elements in \mathbf{j} , p is an integer no less than q . On output, the size of \tilde{U}_q^{-1} is at most $p \times p$, the diagonal entries of \tilde{U}_q^{-1} are all approximately $\frac{1}{\hat{\sigma}}$.

Algorithm 2 Causal Discovery with Latent Variables via Cholesky Factorization (CDCF⁺)

1: **input:** The covariance matrix $\tilde{\Sigma}_{xx} \in \mathbb{R}^{q \times q}$, an estimation $\hat{\sigma}$, and two parameters ζ, μ .
2: **output:** A permutation \tilde{P} and an upper triangular matrix \tilde{U}_q^{-1} .
3: $\underline{j} = []$;
4: **while** $\#\underline{j} \leq p - q$ **do**
5: **call** Alg. 1 with input $\tilde{\Sigma}_{xx}$, output \underline{i} and \tilde{U}_q^{-1} ;
6: **if** $\min_i [\tilde{U}_q^{-1}]_{ii} < \frac{1-\zeta}{\hat{\sigma}}$ **then**
7: $j = \operatorname{argmin}_i [\tilde{U}_q^{-1}]_{ii} < \frac{1-\zeta}{\hat{\sigma}}$;
8: $q = q + 1$;
9: $\underline{j} = [\underline{j}, j]$, $\underline{j}^c = [1, \dots, q] \setminus \underline{j}$;
10: $\underline{i} = [\underline{i}_1, \dots, \underline{i}_{j-1}, q, \underline{i}_j, \dots, \underline{i}_{q-1}]$, $\underline{i}^c = \underline{i}_{\underline{j}^c}$;
11: Solve (17) for \mathbf{S} ;
12: Compute $\mathbf{C}(\mathbf{S})$ in (16);
13: Update $\tilde{\Sigma}_{xx}$ via (18);
14: **else**
15: **break**;
16: **end if**
17: **end while**
18: Set $\tilde{P} = \mathbf{I}(:, \underline{i})$.

Time Complexity. For each “while” loop of CDCF⁺, the time complexity is dominated by line 11; line 5 is simply CDCF and the time complexity is $\mathcal{O}(q^3)$; line 12 is the inversion of an upper triangular matrix and a matrix-matrix multiplication, the time complexity is $\mathcal{O}(q^3)$; the time complexity of the rest can be ignored. Line 11, sub-gradient method is used to solve the optimization problem (17), the time complexities for gradient calculation and updating \mathbf{S} are both $\mathcal{O}(q^2)$. Assume the sub-gradient method needs $\mathcal{O}(\log \frac{1}{\epsilon})$ iterations to solve (17), then the time complexity for Line 11 is $\mathcal{O}(q^2 \log \frac{1}{\epsilon})$. Overall speaking, the time complexity of CDCF⁺ is $\mathcal{O}((p - q)(q + \log \frac{1}{\epsilon})q^2)$.

Convergence. With a proper choice of μ , Algorithm 2 converges in finite steps, and the output \tilde{U}_q^{-1} has almost identical diagonal entries, additionally, due to the ℓ_1 -penalty term, \tilde{U}_q^{-1} is approximately sparse. The proof can be found in the appendix.

Remark 3. Algorithm 2 produces a sparse DAG, but not necessarily the true DAG, since the true DAG with latent variables can be unidentifiable (Adams et al., 2021).

4 Numerical Experiments

In the experiments, the augmented covariance matrix $\tilde{\Sigma}_{xx} = \frac{1}{n} \mathbf{X}^T \mathbf{X} + \lambda \mathbf{I}$ is used to estimate Σ_{xx} , where λ is a parameter.

4.1 Experiments for CDCF

In this section, we present the results of our experiments conducted on simulated graphs, bioinformatics datasets, and knowledge base datasets. Additionally, further experiments addressing non-Gaussian distributions and diagonal augmentation settings are provided in the appendix.

4.1.1 Simulated Graphs

We evaluate CDCF on simulated graphs from two well-known ensembles of random graph types: Erdős–Rényi (ER) (Gilbert, 1959) and Scale-free (SF) (Barabási and Albert, 1999). The average edge number per node is denoted after the graph type, e.g., ER2 represents two edges per node on average. After the graph structure is settled, we assign uniformly random edge weights. We generate the observation data \mathbf{X} from the linear Gaussian SEM.

Our baselines include: NOTEARS (Zheng et al., 2018), DAG-GNN (Yu et al., 2019), CORL (Wang et al., 2021), NPVAR (Gao et al., 2020), and EQVAR (Chen et al., 2019). Other methods such as PC algorithm (Spirtes et al., 2000), LiNGAM (Shimizu et al., 2006), FGS (Ramsey et al., 2017), MMHC (Tsamardinos et al., 2006), LIOBS (Schmidt et al., 2007), CAM (Bühlmann et al., 2014), RL-BIC2 (Zhu et al., 2020), A*LASSO (Xiang and Kim, 2013), LISTEN (Ghoshal and Honorio, 2018), US (Park, 2020) perform no better than the baseline EQVAR.

Table 2: Results of 50, 100, 1000 nodes on 3000 linear Gaussian SEM samples.

Nodes	Graph	NOTEARS	DAG-GNN	CORL-2	NPVAR	EV-TD	CDCF
50	ER2	38.6 _{10.8}	30.6 _{8.3}	17.9 _{10.6}	0.4 _{0.5}	0.0_{0.0}	0.0_{0.0}
	ER5	67.8 _{7.5}	93.2 _{109.4}	64.8 _{13.1}	0.6 _{0.8}	0.1 _{0.3}	0.0_{0.0}
	SF2	3.5 _{1.6}	79.3 _{93.2}	0.0_{0.0}	1.1 _{1.0}	0.0_{0.0}	0.0_{0.0}
	SF5	20.1 _{14.3}	89.2 _{99.2}	20.8 _{10.1}	1.0 _{0.9}	0.0_{0.0}	0.0_{0.0}
100	ER2	72.6 _{23.5}	66.2 _{19.2}	18.6 _{5.7}	2.1 _{1.2}	0.0_{0.0}	0.0_{0.0}
	ER5	170.3 _{34.2}	236.4 _{36.8}	164.8 _{17.1}	2.3 _{1.2}	0.2 _{0.4}	0.1_{0.3}
	SF2	2.3 _{1.3}	156.8 _{21.2}	0.0_{0.0}	3.0 _{1.41}	0.0_{0.0}	0.0_{0.0}
	SF5	90.2 _{34.5}	165.2 _{22.0}	10.8 _{6.1}	2.7 _{0.9}	0.1 _{0.3}	0.0_{0.0}
1000	ER2	-	-	-	-	0.4 _{0.5}	0.1_{0.3}
	ER5	-	-	-	-	21.8 _{3.8}	8.9_{4.2}
	SF2	-	-	-	-	0.0_{0.0}	0.0_{0.0}
	SF5	-	-	-	-	0.3 _{0.5}	0.0_{0.0}

Table 2 presents the structural Hamming distance (SHD) of baseline methods and our method on 3000 samples ($n = 3000$). Nodes number p is noted in the first column. Graph type and edge level are noted in the second column. We only report the SHD of different algorithms due to page limitations. And we find that other metrics such as true positive rate (TPR), false discovery rate (FDR), false positive rate (FPR), and F1 score have similar comparative performance with SHD. We also test bottom-up EQVAR, which is equivalent to LISTEN. The result is worse than top-down EQVAR (EV-TD) in this synthetic experiment, so we do not include the result in the table. For $p = 1000$ graphs, we only report the result of EV-TD and CDCF since other algorithms spend too much time (longer than a week).

We run our methods on 10 randomly generated graphs and report the mean and variance in the table. Figure 2 plots the SHD results tested on 100 nodes graph recovering from different sample sizes. In the low dimension setting ($p < n$), we choose EV-TD, LISTEN (LTN), and LISTEN with Cholesky estimator (LTN-CH) as baselines. In the high dimension setting ($p > n$), we choose high dimension top-down (EV-HTD) and LISTEN (LTN) as baselines. We can see that CDCF achieves significantly better performance compared with previous baselines. In most cases, CDCF can reconstruct the DAG structure exactly according to the observing data, while the other algorithms fail to recover the ground truth graphs.

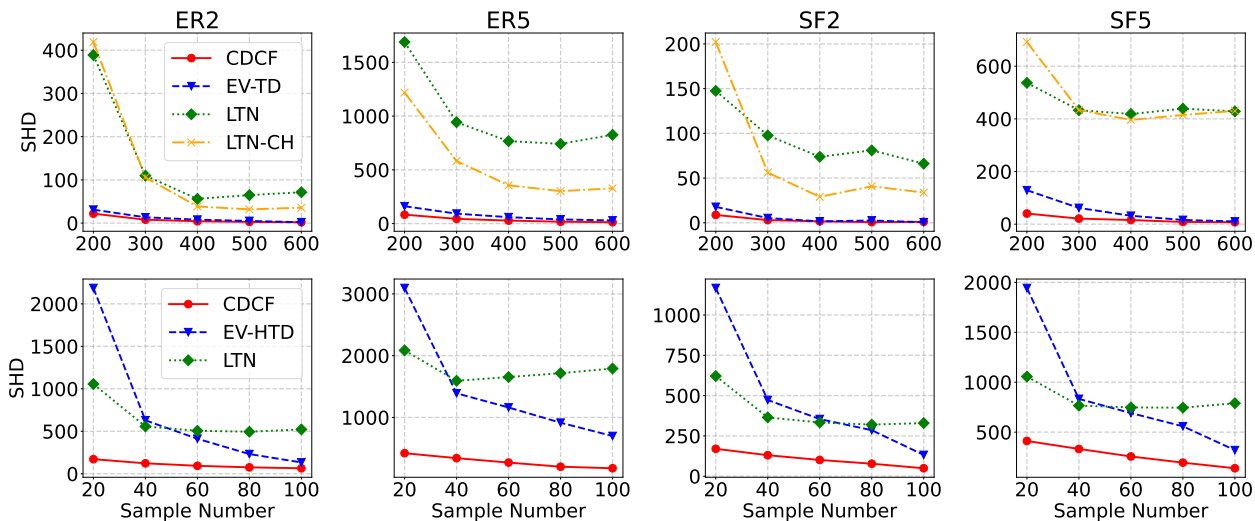


Figure 2: Performance (SHD) tested on 100 nodes graph recovering from different sample numbers.

Table 3: Running time (seconds) on 30 and 100 nodes over 3000 samples.

	30				100			
	ER2	ER5	SF2	SF5	ER2	ER5	SF2	SF5
CDCF	0.004	0.005	0.004	0.005	0.017	0.016	0.016	0.017
EV-TD	0.19	0.16	0.12	0.12	14.42	12.88	15.04	14.78
LISTEN	0.26	0.13	0.13	0.14	13.97	13.41	13.42	15.43
EV-HTD	8.27	7.48	6.72	12.50	260.74	302.36	241.59	387.92
DAG-GNN	49.15	49.02	38.44	41.03	137.25	238.71	158.13	187.21
NPVAR	84.24	82.57	108.37	109.13	9867.96	9084.78	10667.88	10173.89
NOTEARS	78.19	597.16	51.57	306.31	3237.8	1803.30	880.19	4159.82
CORL1	17573.08	18799.21	16422.11	16588.30	—	—	—	—

Table 3 shows the running time, tested on a 2.3 GHz single Intel Core i5 CPU. As illustrated in the table, CDCF is dozens or hundreds of times faster than EV-TD and LISTEN and tens of thousands of times faster than NOTEARS.

4.1.2 Proteins Dataset

We consider a bioinformatics dataset (Sachs et al., 2005) consisting of continuous measurements of expression levels of proteins and phospholipids in the human immune system cells. This is a widely used dataset for research on graphical models, with experimental annotations accepted by the biological research community. Following the previous algorithms setting, we noticed that different previous papers adopted different observations. To included them all, we considered the observational 853 samples from the “CD3, CD28” simulation tested by Teyssier and Koller (2005); Lachapelle et al. (2020); Zhu et al. (2020) and all 7466 samples from nine different simulations tested by Zheng et al. (2018, 2020); Ng et al. (2019).

Table 4: Results on Proteins datasets.

Datasets	Methods	FDR	TPR	FPR	SHD	N	P	F1
853 samples 17 edges	CDCF-V	0.533	0.412	0.210	11	15	0.467	0.438
	CDCF-S	0.500	0.412	0.184	10	14	0.500	0.452
	CDCF-VS	0.500	0.412	0.184	10	14	0.500	0.452
	NOTEARS	0.588	0.412	0.263	13	17	0.412	0.412
	NOTEARSMLP	0.733	0.235	0.290	18	15	0.267	0.250
	CORL1&2	0.533	0.412	0.211	11	15	0.467	0.438
	EV-TD	0.645	0.294	0.237	17	14	0.357	0.323
	LISTEN	0.750	0.176	0.237	18	12	0.250	0.207
	NPVAR	0.800	0.176	0.316	19	15	0.200	0.188
DAG-GNN	0.588	0.412	0.263	15	17	0.412	0.412	
7466 samples 20 edges	CDCF-V	0.667	0.400	0.457	21	24	0.333	0.364
	CDCF-S	0.611	0.350	0.314	17	18	0.389	0.368
	CDCF-VS	0.556	0.400	0.286	16	18	0.444	0.421
	NOTEARS	0.650	0.350	0.371	20	20	0.350	0.350
	NOTEARSMLP	0.800	0.200	0.457	26	20	0.200	0.200
	CORL1&2	0.667	0.400	0.457	21	24	0.333	0.363
	EV-TD	0.700	0.300	0.400	25	20	0.300	0.300
	LISTEN	0.714	0.300	0.429	23	21	0.286	0.293
	NPVAR	0.679	0.450	0.543	24	28	0.321	0.375
DAG-GNN	0.650	0.350	0.371	20	20	0.350	0.350	

We notice that CDCF determines the ordering by the variance (10). One may also take the sparsity into consideration. In fact, we make the three criterion below to introduce sparsity into CDCF. We select i_k according to one of the following criteria:

- (V) $i_k = \operatorname{argmin}_{k \leq j \leq p} \alpha_j^2$. Under the assumption that the noise variance of the child variable is approximately larger than that of its parents, it is reasonable/natural to select the index that has the lowest estimation of the noise variance. This criterion is same with CDCF introduced in Section 2.
- (S) $i_k = \operatorname{argmin}_{k \leq j \leq p} \|\tilde{\mathbf{U}}_{k-1}^{-1} \boldsymbol{\beta}_j\|_1$. When the adjacent matrix \mathbf{T} is sparse, and the noise variables are independent, we would like to select the index that leads to the most sparse column of $\tilde{\mathbf{U}}_k^{-1}$. This criterion is especially useful when the number of samples is small.
- (VS) $i_k = \operatorname{argmin}_{k \leq j \leq p} \|\tilde{\mathbf{U}}_{k-1}^{-1} \boldsymbol{\beta}_j\|_1 \sqrt{|\alpha_j^2 - \frac{1}{k-1} \sum_{h=1}^{k-1} \frac{1}{[\tilde{\mathbf{U}}_{k-1}^{-1}]_{hh}^2}|}$. We empirically combine criterion (V) and criterion (S) together to take both aspects (variance and sparsity) into account. Numerically, we found that this criterion achieves the best performance in real-world data.

We report the experimental results on both settings in Table 4. The evaluation metric is FDR, TPR, FPR, SHD, predicted nodes number (N), precision (P), F1 score. As the recall score equals TPR, we do not include it in the table. In both settings, CDCF-VS achieves state-of-the-art performance.¹ Several reasons make the recovered graph not exactly the same as the expected one.

¹For NOTEARS-MLP, Table 4 reports the results reproduced by the code provided in Zheng et al. (2020).

The ground truth graph suggested by the paper is mixed with directed and indirect edges. Under the settings of SEM, the node “PKA” is quite similar to the leaf nodes since most of its edges are indirect while the ground truth graph notes it as the out edges. Non-linearity would not be an impact issue here since both NOTEARS and our algorithm achieve decent results. In the meantime, we do not deny that further extension of our algorithm to non-linear representation would witness an improvement on this dataset.

4.1.3 Knowledge Base Dataset

We test our algorithm on FB15K-237 dataset (Toutanova et al., 2015) in which the knowledge is organized as $\{Subject, Predicate, Object\}$ triplets. The dataset has 15K triplets and 237 types of predicates. In this experiment, we only consider the single jump predicate between the entities, which have 97 predicates remaining. We want to discover the causal relationships between the predicates. We organize the observation data as each sample corresponds to an entity with awareness of the position (Subject or Object), and each variable corresponds to a predicate in this knowledge base.

In Figure 3, we give the adjacent weighted matrix of the generated graph and several examples with high confidence (larger than 0.5). In the left figure, the axis label notes the first capital letter of the domain of the relations. Some of them are replaced with a dot to save space. Specifically, the axis labels of Figure 3 are ‘Film’, ‘People’, ‘Location’, ‘Music’, ‘Education’, ‘Tv’, ‘Medicine’, ‘Sports’, ‘Olympics’, ‘Award’, ‘Time’, ‘Organization’, ‘Language’, ‘MediaCommon’, ‘Influence’, ‘Dataworld’, ‘Business’, ‘Broadcast’ from left to right for x-axis and top to bottom for y-axis, respectively. The adjacent matrix plotted in the Figure is re-permuted to make the relations in the same domain close to each other. We keep the adjacent matrix inside a domain an upper triangular matrix. Such typology is equivalent to the generated matrix with the original order. The domain clusters are denoted in black boxes at the diagonal of the adjacent matrix. The red boxes denoted the cross-domain relations that are worth paying attention to. Consistent with the innateness of human sense, the recovered relationships inside a domain are denser than those across domains. In the

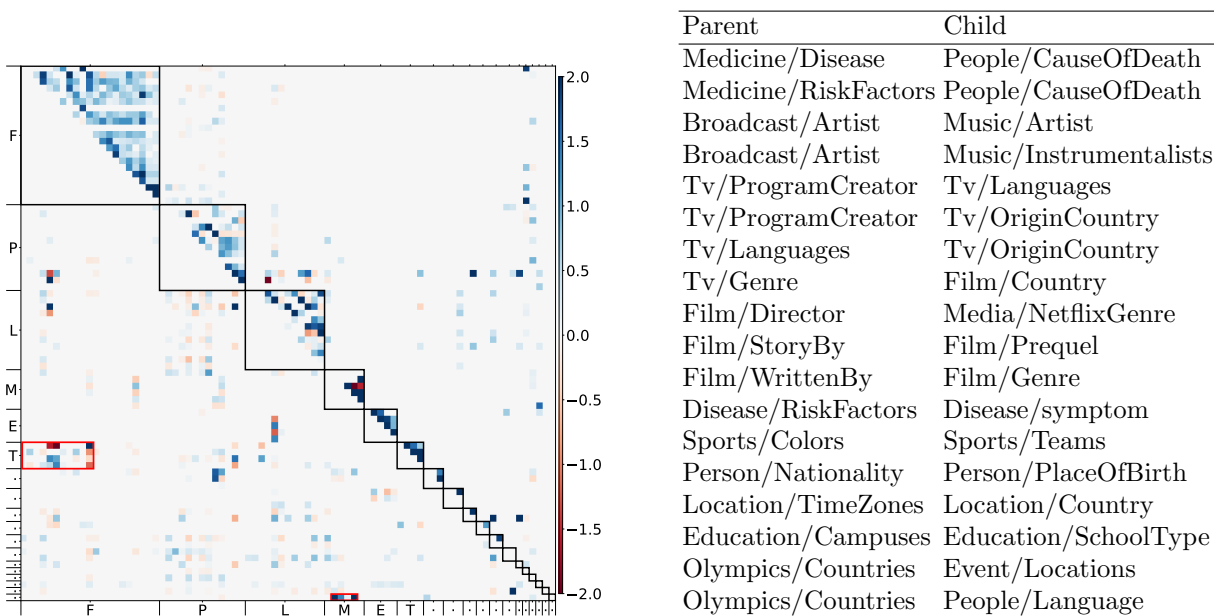


Figure 3: The recovered weighted adjacent matrix (left) and examples of the high confidence relation pairs (right) on FB15k-237 dataset.

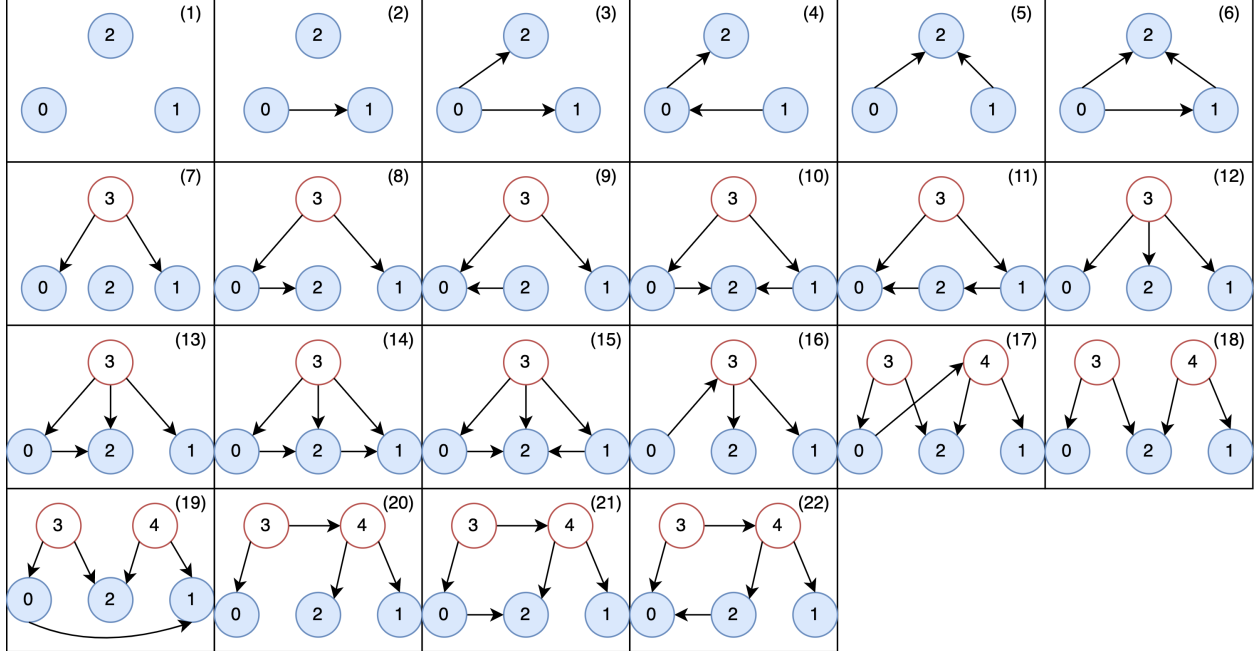


Figure 4: Illustration of 22 identifiable graph types. The solid nodes with numbers 0, 1, 2 represent the observed variables, and the hollow nodes with numbers 3, 4 represent the latent variables.

cross-domain relations, we found that the predicate in domain “TV” (“T”) has many relations with the domain “Film” (“F”), the domain “Broadcast” (last row) have many relations with the domain “Music” (“M”). Several cases of the predicted causal relationships are listed on the right side of Figure 3, we can see that the discovered indication relations between predicates are quite reasonable.

4.2 Experiments for CDCF⁺

We compare CDCF⁺ with BIC guided search (B-S) algorithm mentioned in Adams et al. (2021). Their results show 22 different identifiable (up to re-indexing of the latent variables) typologies with three observable nodes and 0-2 unobservable nodes, which are shown in Figure 4. Following their settings, we test Algorithm 2 on the 22 graphs. We randomly generate 10 datasets for each graph and provide the average results in Table 5. For each random dataset, the result is recorded as the best SHD score among the latent variable permutations.

Table 5: Average SHD on partially observable models.

Sample	Method	Graph Type																					
		1	2	3	4	5	6	7	8	9	10	11	12	13	14	15	16	17	18	19	20	21	22
5e3	B-S	0.0	1.6	1.0	2.2	0.0	3.8	3.0	4.4	3.0	4.6	4.5	3.5	4.6	3.8	6.6	4.6	5.6	6.0	6.1	5.4	5.1	5.7
	OUR	0.0	0.0	0.0	0.0	0.0	0.0	0.0	0.0	0.0	0.0	0.0	0.0	0.0	0.0	0.0	0.0	10.0	0.0	4.8	0.0	1.3	1.8
1e4	B-S	0.1	1.2	1.5	1.2	0.0	4.4	3.0	4.0	3.0	4.8	4.7	5.0	5.0	4.8	6.2	4.3	6.6	6.0	6.0	5.5	5.3	4.2
	OUR	0.0	0.0	0.0	0.0	0.0	0.0	0.0	0.0	0.0	0.0	0.0	0.0	0.0	0.0	0.0	0.0	10.0	0.0	5.0	0.0	1.2	1.9

We compare CDCF⁺ with B-S (Adams et al., 2021), which is the most recent baseline and is applicable to equal variance and Gaussian noise cases without specific topology conditions.

Algorithms like FCI (Spirtes et al., 1999), RFCI (Colombo et al., 2012), and ICD (Rohekar et al., 2021) require specific topology conditions and can only recover the structure up to a partial ancestral graph, which is an equivalence class of the true causal graph, even in the situation that the causal graph is identifiable which is the setting of this experiment. Algorithms like FOFC (Kummerfeld and Ramsey, 2016), BPC (de Andrade e Silva et al., 2006), can only find the causal clusters, i.e., locating latent variables, under the cases when the latent variable have at least three pure measurement variables. Besides, they can not discover the causal order of latent variables.

Table 5 shows that our algorithm achieves significantly better performance and does not depend on the specified latent structures (e.g., confounder, mediator). More experimental details are provided in Appendix.

5 Conclusion

We have proposed two algorithms to tackle the DAG recovery problems with full/partial observations, respectively. The first algorithm CDCF has theoretical guarantees for exact recovery and is better than the existing methods in both time and sample complexities. Experimental results on synthetic datasets and real-world data demonstrate the efficiency and effectiveness of CDCF. The second algorithm CDCF⁺ is able to reveal latent variables and return a sparse DAG. Numerical results indicate that CDCF⁺ recovers most of the topology structures exactly, and the performance is significantly better than previous algorithms. Under what conditions (the “restrictive” assumption **A3** is insufficient) Algorithm 2 is able to produce the true DAG requires a further investigation.

References

- Jeffrey Adams, Niels Hansen, and Kun Zhang. Identification of partially observed linear causal models: Graphical conditions for the non-gaussian and heterogeneous cases. In *Advances in Neural Information Processing Systems (NeurIPS)*, pages 22822–22833, virtual, 2021.
- Bryon Aragam and Qing Zhou. Concave penalized estimation of sparse gaussian bayesian networks. *J. Mach. Learn. Res.*, 16:2273–2328, 2015.
- Albert-László Barabási and Réka Albert. Emergence of scaling in random networks. *Science*, 286(5439):509–512, 1999.
- Peter Bühlmann, Jonas Peters, and Jan Ernest. CAM: Causal additive models, high-dimensional order search and penalized regression. *The Annals of Statistics*, pages 2526–2556, 2014.
- Ruichu Cai, Feng Xie, Clark Glymour, Zhifeng Hao, and Kun Zhang. Triad constraints for learning causal structure of latent variables. In *Advances in Neural Information Processing Systems (NeurIPS)*, pages 12863–12872, Vancouver, Canada, 2019.
- Wenyu Chen, Mathias Drton, and Y Samuel Wang. On causal discovery with an equal-variance assumption. *Biometrika*, 106(4):973–980, 2019.
- David Maxwell Chickering. Optimal structure identification with greedy search. *J. Mach. Learn. Res.*, 3:507–554, 2002.
- Diego Colombo, Marloes H Maathuis, Markus Kalisch, and Thomas S Richardson. Learning high-dimensional directed acyclic graphs with latent and selection variables. *The Annals of Statistics*, pages 294–321, 2012.

- Ricardo Bezerra de Andrade e Silva, Richard Scheines, Clark Glymour, and Peter Spirtes. Learning the structure of linear latent variable models. *J. Mach. Learn. Res.*, 7:191–246, 2006.
- Nir Friedman and Daphne Koller. Being bayesian about network structure. A bayesian approach to structure discovery in bayesian networks. *Mach. Learn.*, 50(1-2):95–125, 2003.
- Ming Gao, Yi Ding, and Bryon Aragam. A polynomial-time algorithm for learning nonparametric causal graphs. In *Advances in Neural Information Processing Systems (NeurIPS)*, virtual, 2020.
- Asish Ghoshal and Jean Honorio. Learning identifiable Gaussian Bayesian networks in polynomial time and sample complexity. In *Advances in Neural Information Processing Systems (NIPS)*, pages 6457–6466, Long Beach, CA, 2017.
- Asish Ghoshal and Jean Honorio. Learning linear structural equation models in polynomial time and sample complexity. In *Proceedings of the International Conference on Artificial Intelligence and Statistics (AISTATS)*, pages 1466–1475, Playa Blanca, Lanzarote, Canary Islands, Spain, 2018.
- Edgar N Gilbert. Random graphs. *The Annals of Mathematical Statistics*, 30(4):1141–1144, 1959.
- Patrik O. Hoyer, Dominik Janzing, Joris M. Mooij, Jonas Peters, and Bernhard Schölkopf. Nonlinear causal discovery with additive noise models. In *Advances in Neural Information Processing Systems (NIPS)*, pages 689–696, Vancouver, Canada, 2008a.
- Patrik O. Hoyer, Shohei Shimizu, Antti J. Kerminen, and Markus Palviainen. Estimation of causal effects using linear non-gaussian causal models with hidden variables. *Int. J. Approx. Reason.*, 49(2):362–378, 2008b.
- Erich Kummerfeld and Joseph D. Ramsey. Causal clustering for 1-factor measurement models. In *Proceedings of the 22nd ACM SIGKDD International Conference on Knowledge Discovery and Data Mining (KDD)*, pages 1655–1664, San Francisco, CA, 2016.
- Sébastien Lachapelle, Philippe Brouillard, Tristan Deleu, and Simon Lacoste-Julien. Gradient-based neural DAG learning. In *Proceedings of the 8th International Conference on Learning Representations (ICLR)*, Addis Ababa, Ethiopia, 2020.
- Hao-Chih Lee, Matteo Danieletto, Riccardo Miotto, Sarah T. Cherng, and Joel T. Dudley. Scaling structural learning with NO-BEARS to infer causal transcriptome networks. In *Proceedings of Pacific Symposium on Biocomputing (PSB)*, pages 391–402, Fairmont Orchid, HI, 2020.
- Yali Lv, Junzhong Miao, Jiye Liang, Ling Chen, and Yuhua Qian. BIC-based node order learning for improving bayesian network structure learning. *Frontiers Comput. Sci.*, 15(6):156337, 2021.
- Brendan D McKay, Frederique E Oggier, Gordon F Royle, NJA Sloane, Ian Murray Wanless, Herbert S Wilf, et al. Acyclic digraphs and eigenvalues of $(0, 1)$ -matrices. *Journal of integer sequences*, 7(2):1–5, 2004.
- Ignavier Ng, Shengyu Zhu, Zhitang Chen, and Zhuangyan Fang. A graph autoencoder approach to causal structure learning. *arXiv preprint arXiv:1911.07420*, 2019.
- Ignavier Ng, Shengyu Zhu, Zhuangyan Fang, Haoyang Li, Zhitang Chen, and Jun Wang. Masked gradient-based causal structure learning. In *Proceedings of the 2022 SIAM International Conference on Data Mining (SDM)*, pages 424–432, Alexandria, VA, 2022.

- Victor A Nicholson. Matrices with permanent equal to one. *Linear Algebra and its Applications*, 12(2):185–188, 1975.
- Xueyan Niu, Xiaoyun Li, and Ping Li. Learning cluster causal diagrams: An information-theoretic approach. In *Proceedings of the Thirty-First International Joint Conference on Artificial Intelligence (IJCAI)*, pages 4871–4877, Vienna, Austria, 2022.
- Gunwoong Park. Identifiability of additive noise models using conditional variances. *J. Mach. Learn. Res.*, 21:75:1–75:34, 2020.
- Jonas Peters, Joris M. Mooij, Dominik Janzing, and Bernhard Schölkopf. Causal discovery with continuous additive noise models. *J. Mach. Learn. Res.*, 15(1):2009–2053, 2014.
- Jonas Peters, Dominik Janzing, and Bernhard Schölkopf. *Elements of causal inference: foundations and learning algorithms*. The MIT Press, 2017.
- Joseph D. Ramsey, Madelyn Glymour, Ruben Sanchez-Romero, and Clark Glymour. A million variables and more: the fast greedy equivalence search algorithm for learning high-dimensional graphical causal models, with an application to functional magnetic resonance images. *Int. J. Data Sci. Anal.*, 3(2):121–129, 2017.
- Shaogang Ren and Ping Li. Flow-based perturbation for cause-effect inference. In *Proceedings of the 31st ACM International Conference on Information & Knowledge Management (CIKM)*, pages 1706–1715, Atlanta, GA, 2022.
- Shaogang Ren, Haiyan Yin, Mingming Sun, and Ping Li. Causal discovery with flow-based conditional density estimation. In *Proceedings of the IEEE International Conference on Data Mining (ICDM)*, pages 1300–1305, Auckland, New Zealand, 2021.
- Shaogang Ren, Belhal Karimi, Dingcheng Li, and Ping Li. Variational flow graphical model. In *Proceedings of the 28th ACM SIGKDD Conference on Knowledge Discovery and Data Mining (KDD)*, pages 1493–1503, Washington, DC, 2022a.
- Shaogang Ren, Dingcheng Li, and Ping Li. Causal effect prediction with flow-based inference. In *Proceedings of the IEEE International Conference on Data Mining (ICDM)*, pages 1167–1172, Orlando, FL, 2022b.
- Raanan Y. Rohekar, Shami Nisimov, Yaniv Gurwicz, and Gal Novik. Iterative causal discovery in the possible presence of latent confounders and selection bias. In *Advances in Neural Information Processing Systems (NeurIPS)*, pages 2454–2465, virtual, 2021.
- Karen Sachs, Omar Perez, Dana Pe’er, Douglas A Lauffenburger, and Garry P Nolan. Causal protein-signaling networks derived from multiparameter single-cell data. *Science*, 308(5721):523–529, 2005.
- Saber Salehkaleybar, AmirEmad Ghassami, Negar Kiyavash, and Kun Zhang. Learning linear non-gaussian causal models in the presence of latent variables. *J. Mach. Learn. Res.*, 21:39:1–39:24, 2020.
- Mark Schmidt, Alexandru Niculescu-Mizil, and Kevin P. Murphy. Learning graphical model structure using l1-regularization paths. In *Proceedings of the Twenty-Second AAAI Conference on Artificial Intelligence (AAAI)*, pages 1278–1283, Vancouver, Canada, 2007.

- Shohei Shimizu, Patrik O. Hoyer, Aapo Hyvärinen, and Antti J. Kerminen. A linear non-gaussian acyclic model for causal discovery. *J. Mach. Learn. Res.*, 7:2003–2030, 2006.
- Shohei Shimizu, Patrik O. Hoyer, and Aapo Hyvärinen. Estimation of linear non-gaussian acyclic models for latent factors. *Neurocomputing*, 72(7-9):2024–2027, 2009.
- Neil JA Sloane. The on-line encyclopedia of integer sequences, 2003.
- Charles Spearman. Pearson’s contribution to the theory of two factors. *British Journal of Psychology*, 19(1):95, 1928.
- Peter Spirtes, Christopher Meek, and Thomas Richardson. An algorithm for causal inference in the presence of latent variables and selection bias. *Computation, causation, and discovery*, 21:1–252, 1999.
- Peter Spirtes, Clark Glymour, and Richard Scheines. *Causation, Prediction, and Search, Second Edition*. Adaptive computation and machine learning. 2000.
- Chandler Squires, Joshua Amaniampong, and Caroline Uhler. Efficient permutation discovery in causal dags. *arXiv preprint arXiv:2011.03610*, 2020.
- Tatsuya Tashiro, Shohei Shimizu, Aapo Hyvärinen, and Takashi Washio. ParCeLiNGAM: A causal ordering method robust against latent confounders. *Neural Comput.*, 26(1):57–83, 2014.
- Marc Teyssier and Daphne Koller. Ordering-based search: A simple and effective algorithm for learning bayesian networks. In *Proceedings of the 21st Conference in Uncertainty in Artificial Intelligence (UAI)*, pages 548–549, Edinburgh, Scotland, 2005.
- Kristina Toutanova, Danqi Chen, Patrick Pantel, Hoifung Poon, Pallavi Choudhury, and Michael Gamon. Representing text for joint embedding of text and knowledge bases. In *Proceedings of the 2015 Conference on Empirical Methods in Natural Language Processing (EMNLP)*, pages 1499–1509, Lisbon, Portugal, 2015.
- Ioannis Tsamardinos, Laura E. Brown, and Constantin F. Aliferis. The max-min hill-climbing bayesian network structure learning algorithm. *Mach. Learn.*, 65(1):31–78, 2006.
- Xiaoqiang Wang, Yali Du, Shengyu Zhu, Liangjun Ke, Zhitang Chen, Jianye Hao, and Jun Wang. Ordering-based causal discovery with reinforcement learning. In *Proceedings of the Thirtieth International Joint Conference on Artificial Intelligence (IJCAI)*, pages 3566–3573, Virtual Event / Montreal, Canada, 2021.
- Jing Xiang and Seyoung Kim. A* lasso for learning a sparse bayesian network structure for continuous variables. In *Advances in Neural Information Processing Systems (NIPS)*, pages 2418–2426, Lake Tahoe, NV, 2013.
- Feng Xie, Ruichu Cai, Biwei Huang, Clark Glymour, Zhifeng Hao, and Kun Zhang. Generalized independent noise condition for estimating latent variable causal graphs. In *Advances in Neural Information Processing Systems (NeurIPS)*, virtual, 2020.
- Qiaoling Ye, Arash A. Amini, and Qing Zhou. Optimizing regularized cholesky score for order-based learning of bayesian networks. *IEEE Trans. Pattern Anal. Mach. Intell.*, 43(10):3555–3572, 2021.

Yue Yu, Jie Chen, Tian Gao, and Mo Yu. DAG-GNN: DAG structure learning with graph neural networks. In *Proceedings of the 36th International Conference on Machine Learning (ICML)*, pages 7154–7163, Long Beach, CA, 2019.

Xun Zheng, Bryon Aragam, Pradeep Ravikumar, and Eric P. Xing. DAGs with NO TEARS: continuous optimization for structure learning. In *Advances in Neural Information Processing Systems (NeurIPS)*, pages 9492–9503, Montréal, Canada, 2018.

Xun Zheng, Chen Dan, Bryon Aragam, Pradeep Ravikumar, and Eric P. Xing. Learning sparse nonparametric DAGs. In *Proceedings of the 23rd International Conference on Artificial Intelligence and Statistics (AISTATS)*, pages 3414–3425, Online [Palermo, Sicily, Italy], 2020.

Rong Zhu, Andreas Pfadler, Ziniu Wu, Yuxing Han, Xiaoke Yang, Feng Ye, Zhenping Qian, Jingren Zhou, and Bin Cui. Efficient and scalable structure learning for bayesian networks: Algorithms and applications. In *Proceedings of the 37th IEEE International Conference on Data Engineering (ICDE)*, pages 2613–2624, Chania, Greece, 2021.

Shengyu Zhu, Ignavier Ng, and Zhitang Chen. Causal discovery with reinforcement learning. In *Proceedings of the 8th International Conference on Learning Representations (ICLR)*, Addis Ababa, Ethiopia, 2020.

A Proofs

Our proofs for Theorems 2.1 and 2.2 are based on the perturbation analysis for the Cholesky factorization of the covariance matrix, the following lemma plays the central role.

Lemma A.1. *Let $\mathbf{x} \in \mathbb{R}^p$ be a zero-mean random vector, $\Sigma_{xx} = \mathbb{E}(\mathbf{x}\mathbf{x}^T) \in \mathbb{R}^{p \times p}$ be the covariance matrix, $\tilde{\Sigma}_{xx}$ be an estimator for Σ_{xx} satisfying that*

$$\max_i |[\Sigma_{xx}]_{ii} - [\tilde{\Sigma}_{xx}]_{ii}| \leq \epsilon_d, \quad \|\Sigma_{xx} - \tilde{\Sigma}_{xx}\| \leq \epsilon_2,$$

for some $\epsilon_d, \epsilon_2 > 0$. Let the Cholesky factorizations of Σ_{xx} and $\tilde{\Sigma}_{xx}$ be $\Sigma_{xx} = \mathbf{U}^T \mathbf{U}$ and $\tilde{\Sigma}_{xx} = \tilde{\mathbf{U}}^T \tilde{\mathbf{U}}$, respectively, where \mathbf{U} and $\tilde{\mathbf{U}}$ are both upper triangular. Then

$$|\|\mathbf{U}_{:,i}\|^2 - \|\tilde{\mathbf{U}}_{:,i}\|^2| \leq \epsilon_d, \quad \text{for } 1 \leq i \leq p; \quad (19)$$

$$|[\mathbf{U}^{-1}]_{ij} - [\tilde{\mathbf{U}}^{-1}]_{ij}| \leq \|\tilde{\mathbf{U}}^{-1}\|_{2,\infty} \|\mathbf{U}^{-T}\|_{2,\infty} \sqrt{2\epsilon_2}, \quad \text{for } i > j. \quad (20)$$

Proof. For all $1 \leq i \leq p$, we have

$$|\|\mathbf{U}_{:,i}\|^2 - \|\tilde{\mathbf{U}}_{:,i}\|^2| = |[\Sigma_{xx}]_{ii} - [\tilde{\Sigma}_{xx}]_{ii}| \leq \epsilon_d, \quad (21)$$

which completes the proof for (19).

Next, we show (20). Let

$$\tilde{\mathbf{U}}\mathbf{U}^{-1} = \mathbf{I} + \mathbf{F}, \quad (\mathbf{I} + \mathbf{F})^T(\mathbf{I} + \mathbf{F}) = \mathbf{I} + \mathbf{E}, \quad (22)$$

where \mathbf{F} is upper triangular. We know that

$$\mathbf{U}^{-1} - \tilde{\mathbf{U}}^{-1} = \tilde{\mathbf{U}}^{-1}\mathbf{F}, \quad (23)$$

$$\mathbf{E} = \mathbf{U}^{-T}\tilde{\mathbf{U}}^T\tilde{\mathbf{U}}\mathbf{U}^{-1} - \mathbf{I} = \mathbf{U}^{-T}(\tilde{\Sigma}_{xx} - \Sigma_{xx})\mathbf{U}^{-1}. \quad (24)$$

Then it follows from (23) that for any $i > j$ it holds that

$$|[\mathbf{U}^{-1}]_{ij} - [\tilde{\mathbf{U}}^{-1}]_{ij}| \leq \|\tilde{\mathbf{U}}^{-1}\|_{2,\infty} \|\mathbf{F}_{1:j,j}\|. \quad (25)$$

It follows from the second equality of (22) that

$$(1 + \mathbf{F}_{jj})^2 + \|\mathbf{F}_{1:j-1,j}\|^2 = 1 + \mathbf{E}_{jj}. \quad (26)$$

Therefore,

$$|\mathbf{F}_{jj}| \leq \sqrt{1 + \mathbf{E}_{jj}} - 1 \stackrel{(a)}{\leq} \sqrt{1 + \|\mathbf{U}^{-\mathbf{T}}\|_{2,\infty}^2 \epsilon_2} - 1 \leq \frac{1}{2} \|\mathbf{U}^{-\mathbf{T}}\|_{2,\infty}^2 \epsilon_2, \quad (27)$$

$$\mathbf{F}_{jj}^2 + \|\mathbf{F}_{1:j-1,j}\|^2 \stackrel{(b)}{\leq} 2|\mathbf{F}_{jj}| + \|\mathbf{U}^{-\mathbf{T}}\|_{2,\infty}^2 \|\tilde{\Sigma}_{xx} - \Sigma_{xx}\| \stackrel{(c)}{\leq} 2\|\mathbf{U}^{-\mathbf{T}}\|_{2,\infty}^2 \epsilon_2, \quad (28)$$

where (a) uses (24) and $\|\Sigma_{xx} - \tilde{\Sigma}_{xx}\|_2 \leq \epsilon$, (b) uses (26), (c) uses (27) and (24) and $\|\Sigma_{xx} - \tilde{\Sigma}_{xx}\| \leq \epsilon_2$. Substituting (28) into (25), we obtain

$$|[\mathbf{U}^{-1}]_{ij} - [\tilde{\mathbf{U}}^{-1}]_{ij}| \leq \|\tilde{\mathbf{U}}^{-1}\|_{2,\infty} \sqrt{\mathbf{F}_{jj}^2 + \|\mathbf{F}_{1:j-1,j}\|^2} \leq \|\tilde{\mathbf{U}}^{-1}\|_{2,\infty} \|\mathbf{U}^{-\mathbf{T}}\|_{2,\infty} \sqrt{2\epsilon_2}.$$

This completes the proof. \square

Theorem 2.1 For the linear SEM model (1), assume (3), **A1** and **A2**. Let $\tilde{\Sigma}_{xx}$ be an estimator for $\Sigma_{xx} = [\mathbb{E}(X_j X_k)]$ and $\max_i |[\Sigma_{xx}]_{ii} - [\tilde{\Sigma}_{xx}]_{ii}| \leq \epsilon_d$ for some $\epsilon_d > 0$. If $\epsilon_d < \frac{\Delta}{4}$, Algorithm 1 recovers the ordering exactly.

Proof. $\tilde{\mathbf{i}} = [\tilde{i}_1, \dots, \tilde{i}_p] = [1, \dots, p] \tilde{\mathbf{P}}$, where $\tilde{\mathbf{P}}$ is the output of Algorithm 1. Denote $\tilde{\mathbf{i}}_k = [\tilde{i}_1, \dots, \tilde{i}_k]$, $\mathbf{U} = \text{diag}(\sigma_{i_1}, \dots, \sigma_{i_p})(\mathbf{I} - \mathbf{T})^{-1}$, $\mathbf{u}_k = \mathbf{U}_{1:k-1,k}$, $\tilde{\mathbf{u}}_k = [\tilde{\mathbf{U}}_p]_{1:k-1,k}$.

In Algorithm 1, we have

$$[\tilde{\Sigma}_{xx}]_{\tilde{\mathbf{i}}, \tilde{\mathbf{i}}} = \tilde{\mathbf{U}}_p^{\mathbf{T}} \tilde{\mathbf{U}}_p. \quad (29)$$

Consider the k th diagonal entries of $[\tilde{\Sigma}_{xx}]_{\tilde{\mathbf{i}}, \tilde{\mathbf{i}}}$. By calculations, we get

$$[\tilde{\Sigma}_{xx}]_{\tilde{i}_k, \tilde{i}_k} = [\tilde{\mathbf{U}}_p]_{kk}^2 + \|\tilde{\mathbf{u}}_k\|^2. \quad (30)$$

Recall (7), we have

$$[\Sigma_{xx}]_{i_k, i_k} = \sigma_{i_k}^2 + \|\mathbf{u}_k\|^2. \quad (31)$$

Next, we show that all root nodes can be found by Algorithm 1. Let $i = i_s$ be a root node, $j = i_t$ be not, by calculations, we have

$$[\tilde{\Sigma}_{xx}]_{jj} \stackrel{(a)}{\geq} [\Sigma_{xx}]_{jj} - \epsilon_d \stackrel{(b)}{=} \sigma_{i_t}^2 + \|\mathbf{u}_t\|^2 - \epsilon_d \stackrel{(c)}{\geq} [\Sigma_{xx}]_{ii} + \sigma_{i_t}^2 - \sigma_{i_s}^2 + \|\mathbf{u}_t\|^2 - \epsilon_d \stackrel{(d)}{\geq} [\tilde{\Sigma}_{xx}]_{ii} + \Delta - 2\epsilon_d \stackrel{(e)}{>} [\tilde{\Sigma}_{xx}]_{ii},$$

where (a) uses Lemma A.1, (b), (c) use (31), (d) uses Lemma A.1, A2, (e) is due to $\epsilon < \frac{1}{2}\Delta$. So we have $\{\tilde{i}_1, \dots, \tilde{i}_{p_1}\} = \{i_1, \dots, i_{p_1}\}$, i.e., all root nodes can be found.

Now assume that Algorithm 1 is able to find the nodes in the first ℓ ($1 \leq \ell < r$) layers, layer by layer, specifically, $\{\tilde{i}_1, \dots, \tilde{i}_{p_1}\} = \{i_1, \dots, i_{p_1}\}$, \dots , $\{\tilde{i}_{p_1+\dots+p_{\ell-1}+1}, \dots, \tilde{i}_{p_1+\dots+p_\ell}\} = \{i_{p_1+\dots+p_{\ell-1}+1}, \dots, i_{p_1+\dots+p_\ell}\}$. We show that all nodes in the $\ell + 1$ st layer can also be found by Algorithm 1. Let $i = i_s$ be a node in the $\ell + 1$ st layer, $j = i_t$ be not. We have

$$\begin{aligned} [\tilde{\Sigma}_{xx}]_{jj} - \|[\tilde{\mathbf{u}}_t]_{1:j}\|^2 &\stackrel{(f)}{\geq} [\Sigma_{xx}]_{jj} - \|[\mathbf{u}_t]_{1:j}\|^2 - 2\epsilon_d \stackrel{(g)}{=} \sigma_{i_t}^2 + \|\mathbf{u}_t\|^2 - \|[\mathbf{u}_t]_{1:j}\|^2 - 2\epsilon_d \\ &= \sigma_{i_t}^2 + \|[\mathbf{u}_t]_{j+1:t-1}\|^2 - 2\epsilon_d \stackrel{(h)}{\geq} \sigma_{i_s}^2 + \Delta - 2\epsilon_d \stackrel{(i)}{=} [\Sigma_{xx}]_{ii} - \|\mathbf{u}_s\|^2 + \Delta - 2\epsilon_d \\ &\stackrel{(j)}{\geq} [\tilde{\Sigma}_{xx}]_{ii} - \|\tilde{\mathbf{u}}_s\|^2 + \Delta - 4\epsilon_d \stackrel{(k)}{>} [\tilde{\Sigma}_{xx}]_{ii} - \|\tilde{\mathbf{u}}_s\|^2, \end{aligned}$$

where (f), (j) use Lemma A.1, (g), (i) use (31), (h) uses A2, (k) is due to $\epsilon < \frac{1}{4}\Delta$. So all nodes in the $\ell + 1$ st layer can be found. By mathematical induction, we get the conclusion. \square

Theorem 2.2 Follow the notations and assumptions in Theorem 2.1. Denote

$$\mu = \|\mathbf{I} - \mathbf{T}\|_{2,\infty} \|\mathbf{I} - \mathbf{T}^\top\|_{2,\infty}, \quad \rho = \frac{\max_i \sigma_i}{\min_i \sigma_i^2}, \quad \omega = \min_{\mathbf{T}_{ij} \neq 0} |\mathbf{T}_{ij}|$$

Assume $\|\Sigma_{xx} - \tilde{\Sigma}_{xx}\| \leq \epsilon_2$ for some $\epsilon_2 > 0$. If $\epsilon_2 \lesssim \frac{\omega^2}{8\mu^2\rho^2}$, then Algorithm 1 recovers the graph structure exactly.

Proof. Recall that

$$\mathbf{P}^\top \Sigma_{xx} \mathbf{P} = \mathbf{U}^\top \mathbf{U}, \quad \tilde{\mathbf{P}}^\top \tilde{\Sigma}_{xx} \tilde{\mathbf{P}} = \tilde{\mathbf{U}}_p^\top \tilde{\mathbf{U}}_p,$$

where $\mathbf{U} = \mathbf{P}^\top \Sigma_{nn}^{\frac{1}{2}} \mathbf{P} (\mathbf{I} - \mathbf{T})^{-1}$. Rewrite the first equality as

$$\tilde{\mathbf{P}}^\top \Sigma_{xx} \tilde{\mathbf{P}} = \tilde{\mathbf{P}}^\top \mathbf{P} \mathbf{P}^\top \Sigma_{xx} \mathbf{P} \tilde{\mathbf{P}} = (\mathbf{\Pi}^\top \mathbf{U}^\top \mathbf{\Pi}) (\mathbf{\Pi}^\top \mathbf{U} \mathbf{\Pi}), \quad (32)$$

where $\mathbf{\Pi} = \mathbf{P}^\top \tilde{\mathbf{P}}$. By Lemma A.1, $\mathbf{\Pi}$ is block diagonal and corresponds with the within layer permutation. Recall the structure of \mathbf{T} in (4), we know that $\mathbf{\Pi}^\top \mathbf{U} \mathbf{\Pi}$ is upper triangular, which implies that (32) is a Cholesky factorization. Then it follows from Lemma A.1 that

$$\|\tilde{\mathbf{U}}_q^{-1} - (\mathbf{\Pi}^\top \mathbf{U} \mathbf{\Pi})^{-1}\|_{\max} \leq \|\tilde{\mathbf{U}}_p^{-1}\|_{2,\infty} \|\mathbf{U}^{-\top}\|_{2,\infty} \sqrt{2\epsilon_2}.$$

Since $\tilde{\mathbf{U}}_p^{-1} \rightarrow \mathbf{U}^{-1}$ as $\epsilon_2 \rightarrow 0$, we have $\mathbf{A} := \mathbf{\Pi} \text{diag}(\tilde{\mathbf{U}}_p^{-1}) \mathbf{\Pi}^\top \rightarrow \text{diag}(\sigma_{i_1}^{-1}, \dots, \sigma_{i_p}^{-1})$, and

$$\|\tilde{\mathbf{U}}_q^{-1} - \mathbf{\Pi}^\top \mathbf{U}^{-1} \mathbf{\Pi}\|_{\max} \lesssim \|\mathbf{U}^{-1}\|_{2,\infty} \|\mathbf{U}^{-\top}\|_{2,\infty} \sqrt{2\epsilon_2} \leq \frac{1}{\min_i \sigma_i^2} \|\mathbf{I} - \mathbf{T}\|_{2,\infty} \|\mathbf{I} - \mathbf{T}^\top\|_{2,\infty} \sqrt{2\epsilon_2} = \frac{\mu}{\min_i \sigma_i^2} \sqrt{2\epsilon_2}.$$

Then it follows that

$$\|\mathbf{\Pi} \text{TRIU}(\tilde{\mathbf{U}}_p^{-1}) \mathbf{\Pi}^\top - \mathbf{T} \text{diag}(\sigma_{i_1}^{-1}, \dots, \sigma_{i_p}^{-1})\|_{\max} \lesssim \frac{\mu}{\min_i \sigma_i^2} \sqrt{2\epsilon_2}.$$

And hence

$$\|\mathbf{\Pi} \text{TRIU}(\tilde{\mathbf{U}}_p^{-1} \mathbf{A}) \mathbf{\Pi}^\top - \mathbf{T}\|_{\max} \lesssim \mu \rho \sqrt{2\epsilon_2}.$$

Let $\mu \rho \sqrt{2\epsilon_2} < \frac{\omega}{2}$, we can recover the graph structure by truncating $\text{TRIU}(\tilde{\mathbf{U}}_q^{-1} \mathbf{A})$. The proof is completed. \square

Proof of the sample complexity for exact ordering recovery. Denote $\mathcal{M} = \max_i [\boldsymbol{\Sigma}_{xx}]_{ii}$. Assume $\Delta = \mathcal{O}(1)$. For the random variable X_i^2 , we have $0 \leq \mathbb{E}(X_i^2) \leq \mathcal{M} < \infty$. By Hoeffding's inequality, we get

$$\mathbb{P}(|[\tilde{\boldsymbol{\Sigma}}_{xx}]_{ii} - [\boldsymbol{\Sigma}_{xx}]_{ii}| > t) \leq 2 \exp\left(-\frac{2nt^2}{\mathcal{M}^2}\right).$$

Set $\epsilon = 2 \exp\left(-\frac{2nt^2}{\mathcal{M}^2}\right)$ and $t = \frac{\Delta}{4}$, we get $n = \mathcal{O}(\mathcal{M}^2 \log \frac{1}{\epsilon})$. In other words, w.p. $\geq 1 - \epsilon$, $|[\tilde{\boldsymbol{\Sigma}}_{xx}]_{ii} - [\boldsymbol{\Sigma}_{xx}]_{ii}| \leq \frac{\Delta}{4}$ for $n = \mathcal{O}(\mathcal{M}^2 \log \frac{1}{\epsilon})$. Therefore, w.p. $\geq 1 - \epsilon$, for all $1 \leq i \leq p$, $|[\tilde{\boldsymbol{\Sigma}}_{xx}]_{ii} - [\boldsymbol{\Sigma}_{xx}]_{ii}| \leq \frac{\Delta}{4}$ for $n = \mathcal{O}(\mathcal{M}^2 \log \frac{p}{\epsilon})$. The conclusion follows.

It is worth mentioning here that if we assume $\Delta = \mathcal{O}(\mathcal{M})$ instead, the \mathcal{M} factor in the sample complexity can be removed.

Proof of the sample complexity for exact graph structure recovery. When the noise is sub-Gaussian, it holds with probability at least $1 - 2 \exp(-ct^2)$ that

$$\|\tilde{\boldsymbol{\Sigma}}_{xx} - \boldsymbol{\Sigma}_{xx}\| \leq \|(\mathbf{I} - \mathbf{T})^{-1}\|^2 \max\{\delta, \delta^2\},$$

where $\delta = C\sqrt{\frac{p}{n}} + \frac{t}{\sqrt{n}}$, c and C are two constants. For simplicity, let $\delta \geq 1$. Set $2 \exp(-ct^2) = \epsilon$, we get

$$t = \mathcal{O}\left(\sqrt{\log \frac{1}{\epsilon}}\right), \quad \delta = \mathcal{O}\left(\sqrt{\frac{p}{n}} + \sqrt{\frac{1}{n} \log \frac{1}{\epsilon}}\right).$$

Then w.p. $\geq 1 - \epsilon$, it holds

$$\|\tilde{\boldsymbol{\Sigma}}_{xx} - \boldsymbol{\Sigma}_{xx}\| \leq \|(\mathbf{I} - \mathbf{T})^{-1}\|^2 \delta^2 \leq \|(\mathbf{I} - \mathbf{T})^{-1}\|^2 \mathcal{O}\left(\frac{p + \log \frac{1}{\epsilon}}{n}\right).$$

Let the right hand side be no more than $\frac{\omega^2}{8\mu^2\rho^2}$, we get $n \geq \mathcal{O}\left((p + \log \frac{1}{\epsilon})\rho^2\mu^2\|(\mathbf{I} - \mathbf{T})^{-1}\|^2/\omega^2\right)$. Sample complexities for other distributions of the noise can be obtained similarly.

Proof of Proposition 1. Direct calculations give rise to (a) and (b). Next, we only show (c).

Using $\mathbf{L}^T \mathbf{L} = \mathbf{I} + \mathbf{w}\mathbf{w}^T$, we have

$$\prod_{i=1}^k L_{ii}^2 = \det([\mathbf{L}^T \mathbf{L}]_{1:k,1:k}) = \det(\mathbf{I} + \mathbf{w}_{1:k} \mathbf{w}_{1:k}^T) = 1 + \mathbf{w}_{1:k}^T \mathbf{w}_{1:k} = 1 + \|\mathbf{w}_{1:k}\|^2.$$

Note that, for any nonzero vector $\mathbf{x} \in \mathbb{R}^p$, it holds $(\mathbf{I} + \mathbf{x}\mathbf{x}^T)\mathbf{x} = (1 + \|\mathbf{x}\|^2)\mathbf{x}$, $(\mathbf{I} + \mathbf{x}\mathbf{x}^T)\mathbf{y} = \mathbf{y}$ for any $\mathbf{y}^T \mathbf{x} = 0$. In other words, the eigenvalues of $\mathbf{I} + \mathbf{x}\mathbf{x}^T$ are $1 + \|\mathbf{x}\|^2, 1, \dots, 1$. Therefore, $\det(\mathbf{I} + \mathbf{x}\mathbf{x}^T) =$ the product of all eigenvalues $= 1 + \|\mathbf{x}\|^2$. The conclusion follows immediately.

Convergence of Algorithm 2. In Proposition 2, set the diagonal entries of $\widehat{\mathbf{U}}_{22}$ to $\widehat{\sigma}$, then one can construct a unique vector \mathbf{w} and an upper triangular matrix \mathbf{L} with $V_{ii} = [\mathbf{U}_{22}]_{ii}/\widehat{\sigma}$ for all i such that $\mathbf{L}^T \mathbf{L} = \mathbf{I} + \mathbf{w}\mathbf{w}^T$. Set $\widehat{\mathbf{U}}_{22} = \mathbf{L}^{-1} \mathbf{U}_{22}$, we know that the diagonal entries of $\widehat{\mathbf{U}}_{22}$ are all $\widehat{\sigma}$. Therefore, let j, \mathbf{i} be the same as in Lines 7 and 10 of Algorithm 2, respectively, we know that we can invert one row and column into $\tilde{\boldsymbol{\Sigma}}_{xx}$ such that the diagonal entries of the Cholesky factor of $[\tilde{\boldsymbol{\Sigma}}_{xx}]_{\mathbf{i},\mathbf{i}}$, denoted by $\alpha_1, \dots, \alpha_q$, satisfy

$$\frac{1}{\alpha_i} \geq \frac{1 - \zeta}{\widehat{\sigma}}, \quad \text{for } i = 1, \dots, j - 1; \quad \frac{1}{\alpha_i} = \frac{1}{\widehat{\sigma}} > \frac{1 - \zeta}{\widehat{\sigma}}, \quad \text{for } i = j, \dots, q. \quad (33)$$

By continuity of the optimization problem (17) w.r.t. μ , we take $\alpha_1, \dots, \alpha_q$ as functions of μ . For $\mu = 0$, (17) has a solution \mathbf{S} such that (33) holds. So, for a sufficiently small μ , (17) has a solution \mathbf{S} such that

$$\frac{1}{\alpha_i} \geq \frac{1-\zeta}{\hat{\sigma}}, \quad \text{for } i = 1, \dots, j-1; \quad \frac{1}{\alpha_i} > \frac{1-\zeta}{\hat{\sigma}}, \quad \text{for } i = j, \dots, q. \quad (34)$$

This completes the proof.

B Additional Experiments

B.1 Further Experiments on CDCF

Experiments with non-Gaussian Noise Figure 5 and Figure 6 provide the results of Gumbel and Exponential noises, respectively. As we can see from the result, our algorithm still performs better than the Eqvar method in different noise types.

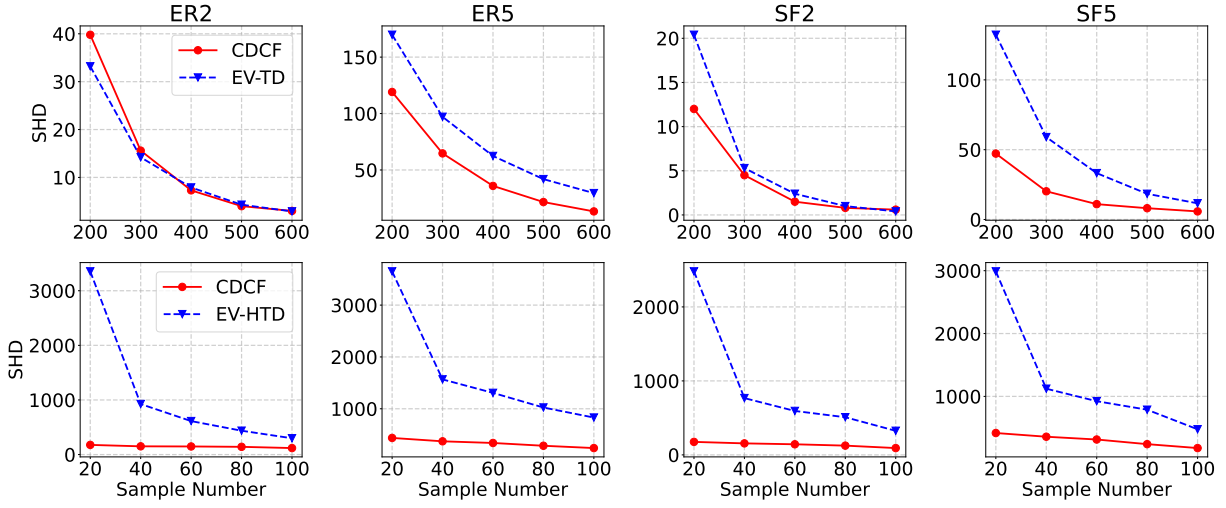


Figure 5: Performance (SHD) on a 100-node graph, with the gumbel noise.

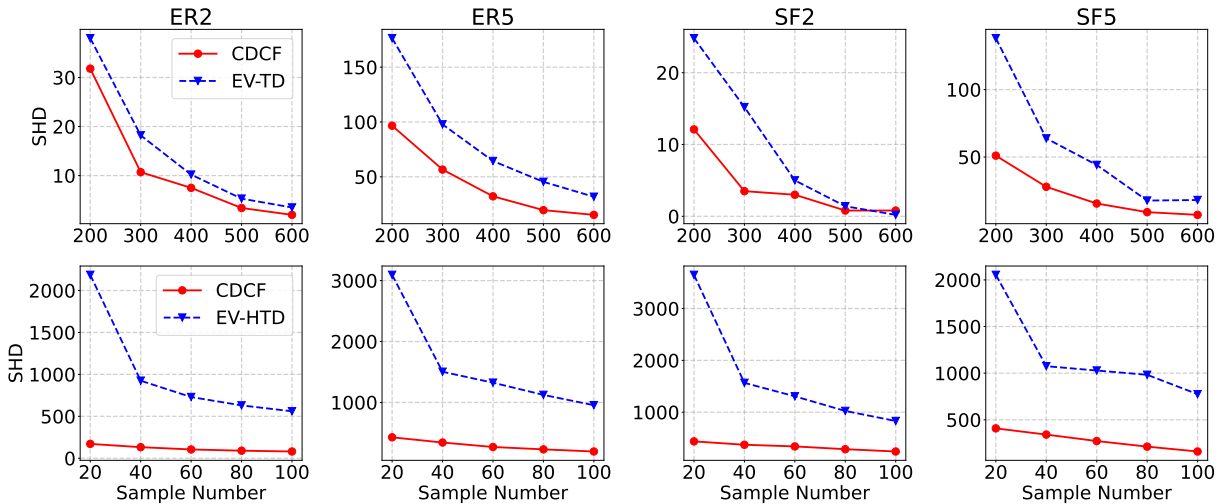


Figure 6: Performance (SHD) on 100 nodes graph, with the exponential noise.

Table 6: CDCF SHD results on with varying γ and sample sizes on 100 nodes linear Gaussian SEM.

	CDCF	200	300	400	500	600	700	800	900	1000	1500	2000	2500	3000
ER2	$\gamma = 0.0$	114.3	32.2	11.7	4.6	2.5	1.4	1.1	0.5	0.4	0.3	0.0	0.0	0.0
	$\gamma = 1.0$	21.9	7.9	4.3	2.8	2.0	1.3	1.4	0.5	0.4	0.3	0.0	0.0	0.0
	$\gamma = 2.0$	13.6	7.2	4.0	2.9	2.1	1.7	1.4	0.9	0.7	0.3	0.0	0.0	0.0
	$\gamma = 3.0$	14.8	8.1	4.5	3.5	2.7	2.0	1.8	1.4	0.7	0.3	0.0	0.0	0.0
	$\gamma = 4.0$	18.3	9.9	7.2	4.9	3.1	3.0	2.3	1.4	0.8	0.6	0.0	0.0	0.0
	$\gamma = 5.0$	23.0	12.3	9.3	6.5	4.1	3.8	2.4	1.6	1.0	0.8	0.1	0.0	0.0
	$\gamma = 6.0$	27.0	14.9	11.4	7.7	4.5	4.4	3.6	1.9	1.7	0.8	0.1	0.1	0.0
	$\gamma = 7.0$	33.0	19.1	13.7	9.1	6.0	4.9	4.3	2.5	2.4	0.9	0.2	0.1	0.0
	$\gamma = 8.0$	37.3	22.1	15.5	10.2	7.0	5.7	5.1	2.9	3.1	1.2	0.2	0.1	0.0
	$\gamma = 9.0$	42.5	25.1	17.6	11.6	8.6	6.9	5.8	3.6	3.4	1.2	0.2	0.1	0.1
$\gamma = 10.0$	46.7	27.4	20.0	12.8	10.0	7.5	6.6	4.5	3.7	1.3	0.3	0.1	0.1	
SF2	$\gamma = 0.0$	37.1	7.2	1.9	2.6	0.9	0.3	0.1	0.1	0.2	0.0	0.0	0.0	0.0
	$\gamma = 1.0$	8.8	3.0	1.6	0.7	1.1	0.5	0.2	0.2	0.1	0.0	0.0	0.0	0.0
	$\gamma = 2.0$	9.7	4.2	2.2	0.9	1.2	0.5	0.2	0.1	0.1	0.0	0.0	0.0	0.0
	$\gamma = 3.0$	11.5	6.2	2.9	1.4	1.2	0.4	0.3	0.1	0.1	0.0	0.0	0.0	0.0
	$\gamma = 4.0$	15.4	7.5	3.5	1.8	1.6	0.8	0.4	0.3	0.2	0.0	0.0	0.0	0.0
	$\gamma = 5.0$	18.1	8.9	4.3	2.7	2.1	1.3	0.5	0.5	0.4	0.0	0.0	0.0	0.0
	$\gamma = 6.0$	20.9	10.8	5.4	3.3	2.5	1.7	0.8	1.0	0.6	0.0	0.0	0.0	0.0
	$\gamma = 7.0$	23.5	13.1	6.7	5.2	4.9	2.7	1.5	1.3	0.7	0.0	0.0	0.0	0.0
	$\gamma = 8.0$	27.0	14.8	8.1	5.8	6.0	2.9	2.2	1.5	0.7	0.0	0.0	0.0	0.0
	$\gamma = 9.0$	29.4	16.8	9.8	6.7	6.7	3.5	2.7	2.0	1.1	0.0	0.0	0.0	0.0
$\gamma = 10.0$	32.0	19.0	11.5	7.4	7.7	4.1	3.0	2.3	1.5	0.1	0.0	0.0	0.0	
ER5	$\gamma = 0.0$	368.7	139.6	73.8	33.2	21.5	14.0	9.5	7.0	5.8	1.5	0.6	0.0	0.0
	$\gamma = 1.0$	83.0	44.2	27.8	17.5	12.5	9.2	7.0	5.1	4.7	1.3	0.7	0.0	0.1
	$\gamma = 2.0$	74.1	41.7	26.2	19.8	13.4	10.7	8.4	6.6	5.7	1.3	1.1	0.0	0.3
	$\gamma = 3.0$	82.1	52.3	33.1	23.0	18.2	14.5	11.9	8.0	7.2	2.4	1.6	0.2	0.4
	$\gamma = 4.0$	94.8	62.1	40.1	28.6	23.9	18.1	14.3	10.3	10.3	3.9	2.1	0.4	0.3
	$\gamma = 5.0$	109.7	72.3	51.4	37.6	30.1	22.6	17.6	14.1	12.8	5.6	2.6	0.8	0.4
	$\gamma = 6.0$	123.3	84.2	57.9	47.8	34.7	26.3	21.2	17.4	15.4	6.7	3.2	0.9	0.5
	$\gamma = 7.0$	140.3	100.2	67.9	53.1	39.9	31.2	25.0	20.2	18.2	7.8	3.7	1.0	0.7
	$\gamma = 8.0$	152.7	113.0	74.8	61.5	47.5	36.4	31.0	23.5	22.3	9.4	4.4	1.4	0.9
	$\gamma = 9.0$	162.5	122.0	83.1	67.7	51.6	42.3	34.6	28.5	25.7	10.7	4.9	1.9	1.4
$\gamma = 10.0$	175.5	130.2	92.6	73.8	59.0	48.8	37.7	33.2	28.7	12.5	5.7	2.4	1.8	
SF5	$\gamma = 0.0$	92.6	31.9	12.6	6.0	4.9	3.9	2.5	1.8	1.6	0.3	0.4	0.0	0.0
	$\gamma = 1.0$	40.3	21.0	15.6	8.3	7.2	5.3	4.1	2.3	2.8	0.5	0.4	0.0	0.0
	$\gamma = 2.0$	57.2	35.7	23.3	16.1	11.2	9.6	7.5	5.9	5.1	1.7	0.6	0.0	0.0
	$\gamma = 3.0$	69.8	46.2	31.3	23.6	16.9	12.5	11.2	8.6	7.0	2.8	1.4	0.0	0.1
	$\gamma = 4.0$	80.9	53.1	38.7	30.4	21.1	17.9	14.5	11.9	8.4	4.2	2.1	0.9	0.2
	$\gamma = 5.0$	90.6	66.3	43.7	36.3	25.8	24.5	20.3	16.6	12.1	5.7	3.3	1.6	0.4
	$\gamma = 6.0$	103.3	73.3	49.1	42.3	34.6	28.1	25.5	19.7	14.4	8.3	4.0	2.4	1.5
	$\gamma = 7.0$	110.3	79.4	55.9	45.6	38.0	31.6	29.1	24.6	19.9	10.3	5.1	3.6	2.1
	$\gamma = 8.0$	118.4	86.1	63.6	50.2	41.3	35.7	33.5	27.6	21.4	12.6	5.8	4.3	2.5
	$\gamma = 9.0$	124.0	92.8	68.7	54.1	46.5	39.4	36.3	30.2	25.0	13.9	7.2	4.7	3.2
$\gamma = 10.0$	129.5	98.6	74.3	57.8	49.6	42.2	39.3	32.6	27.1	17.5	7.7	5.9	4.0	

Experiment on diagonal augmentation parameter. We set the diagonal augmentation parameter $\lambda = \gamma \frac{\log(p)}{n}$. The main result given in the Table 2 and Figure 2 is tested with $\gamma = 1.0$. We give the results in Table 6 on different choices of γ .

B.2 Experiments Details with Unobserved Variables Settings

Data Generation. Given the graph topology, we generate the dataset by linear SEM with equal variance Gaussian noise. The noise variance is set to 1.0, and the edge weight is set to 1.0.

Hyper Parameters. We adopted Adam optimizer with learning rate initialized as 0.05, and decays every 100 gradient step with exponential scheduler with rate 0.99. The sparse loss coefficient μ is 0.05. The trainable parameters \mathbf{S} are initialized as 0.5. For each latent variable, we take the result when the covariance loss less than 0.005 or at most 10 thousand gradient steps. The rounding threshold is set to 0.4. The results tested on different settings of hyperparameters (see Table 7 for details) are given in Table 8. We can see from the table that the performance is not quite sensitive to the hyperparameters for most of the graph types.

Table 7: Parameter suites

Parameter Suite	Optimizer	Learning Rate	Scheduler	μ	ζ	Sample (K)
A	Adam	0.05	0.99/100	0.05	0.1	5
B	Adam	0.05	0.99/100	0.1	0.1	5
C	Adam	0.05	0.99/100	0.05	0.05	5
D	Adam	0.05	0.90/100	0.05	0.05	5
E	SGD	0.005	0.99/100	0.01	0.05	5
F	Adam	0.05	0.99/100	0.05	0.1	10
G	Adam	0.05	0.99/100	0.1	0.1	10
H	Adam	0.05	0.99/100	0.05	0.05	10
I	Adam	0.05	0.90/100	0.05	0.05	10
J	SGD	0.005	0.99/100	0.01	0.05	10
K	Adam	0.05	0.99/100	0.1	0.1	50

Table 8: SHD results on latent variables. Tested on different parameter suites.

Parameter Suite	Graph Type																					
	1	2	3	4	5	6	7	8	9	10	11	12	13	14	15	16	17	18	19	20	21	22
A	0.0	0.0	0.0	0.0	0.0	0.0	0.0	0.0	0.0	0.0	0.0	0.0	0.0	0.0	0.0	0.0	10.0	0.0	4.8	0.0	1.3	1.8
B	0.0	0.0	0.0	0.0	0.0	0.0	0.0	0.0	0.0	0.0	0.0	0.0	4.8	0.0	0.0	0.0	9.5	0.0	4.8	0.0	0.9	3.7
C	0.0	0.0	0.0	0.0	0.0	0.0	0.0	0.0	0.0	0.0	0.0	0.0	1.1	0.0	0.0	0.0	3.4	0.0	4.0	0.0	1.9	1.9
D	0.0	0.0	0.0	0.0	0.0	0.0	0.0	0.0	0.0	0.0	0.0	0.0	0.0	0.0	0.0	0.0	2.9	0.0	3.9	0.0	2.1	2.2
E	0.0	0.0	0.0	0.0	0.0	0.0	0.0	0.0	0.0	0.0	0.0	0.0	3.5	0.0	0.0	2.0	10.0	0.0	3.0	2.0	9.8	7.0
F	0.0	0.0	0.0	0.0	0.0	0.0	0.0	0.0	0.0	0.0	0.0	0.0	0.0	0.0	0.0	0.0	10.0	0.0	5.0	0.0	1.2	1.9
G	0.0	0.0	0.0	0.0	0.0	0.0	0.0	0.0	0.0	0.0	0.0	0.0	0.9	0.0	0.0	0.0	10.0	0.0	4.7	0.0	0.9	3.4
H	0.0	0.0	0.0	0.0	0.0	0.0	0.0	0.0	0.0	0.0	0.0	0.0	0.0	0.0	0.0	0.0	3.0	0.0	3.9	0.0	1.3	1.3
I	0.0	0.0	0.0	0.0	0.0	0.0	0.0	0.0	0.0	0.0	0.0	0.0	0.0	0.0	0.0	0.0	2.6	0.0	4.0	0.0	1.3	2.8
J	0.0	0.0	0.0	0.0	0.0	0.0	0.0	0.0	0.0	0.0	0.0	0.0	5.2	0.0	0.0	2.0	8.0	0.0	2.0	1.9	3.7	7.5
K	0.0	0.0	0.0	0.0	0.0	0.0	0.0	0.0	0.0	0.0	0.0	0.0	0.0	0.0	0.0	0.0	10.0	0.0	3.8	0.0	0.0	1.7

B.3 Baseline Implementations

The baselines are implemented via the codes provided from the following links:

- NOTEARS, NOTEARS-MLP: <https://github.com/xunzheng/notears>
- NPVAR: <https://github.com/MingGao97/NPVAR>
- EQVAR, LISTEN: <https://github.com/WY-Chen/EqVarDAG>
- CORL: <https://github.com/huawei-noah/trustworthyAI/tree/master/gcastle>
- DAG-GNN: <https://github.com/fishmoon1234/DAG-GNN>
- B-S <https://proceedings.neurips.cc/paper/2021/file/c0f6fb5d3a389de216345e490469145e-Supplemental.zip>